The Role of Resonant Coupling in Vibrational Sum-Frequency-Generation Spectroscopy: Liquid Acetonitrile at the Silica Interface

Amanda J. Souna[a,†], Samuel R. Cohen[a,1,†], Christopher A. Rivera[a,2], Katherine Manfred[a,3], Benoit Coasne[b], and John T. Fourkas[a,c,d,e,*]

[a]Department of Chemistry & Biochemistry, University of Maryland, College Park, 20742, USA
[b]Université Grenoble Alpes, CNRS, LIPhy, 38000 Grenoble, France
[c]Institute for Physical Science and Technology, University of Maryland, College Park, 20742, USA
[d]Maryland NanoCenter, University of Maryland, College Park, 20742, USA
[e]Maryland Quantum Materials Center, University of Maryland, College Park, 20742, USA

[1]Present addresses: Department of Biomedical Engineering and Center for Biomolecular Condensates and Center of Regenerative Medicine, Washington University in St. Louis, St. Louis, MO 63130
[2]Present address: nLIGHT Inc., 5408 NE 88th Street, Bldg E, Vancouver, WA 98665
[3]Present address: Wolfson Atmospheric Chemistry Laboratories, Department of Chemistry, University of York, Heslington, York YO10 5DD, North Yorkshire, United Kingdom

†These authors contributed equally to this work

*Corresponding author at Department of Chemistry & Biochemistry, University of Maryland, College Park, 20742, USA (J. T. Fourkas)

E-mail address: benoit.coasne@univ-grenoble-alpes.fr (B. Coasne), fourkas@umd.edu (J. T. Fourkas)

Abstract. Vibrational sum-frequency-generation (VSFG) spectroscopy is a versatile technique for probing molecular organization at interfaces. There is a growing recognition that dynamic phenomena, such as reorientation and intermolecular vibrational coupling, can also influence VSFG spectra. The silica/liquid acetonitrile interface is a useful system for exploring these effects in more detail. The organization of acetonitrile at this interface has been well studied, and is known to resemble that of a supported lipid bilayer in many ways. Here isotopic dilution is used to explore the influence of resonant intermolecular coupling of methyl symmetric stretches on the VSFG spectroscopy of this system. VSFG spectra in the methyl stretching region at this interface show a blue shift, a decrease in linewidth, and a higher-than-expected intensity upon dilution in deuterated acetonitrile. We demonstrate that resonant coupling influences VSFG spectral shifts through the infrared transition. Using molecular simulations, we show that our experimental observations are consistent with resonant coupling between methyl transition dipoles being a significant, but not the dominant, contribution to the observed spectral shift upon isotopic dilution. Furthermore, our molecular simulations demonstrate that resonant coupling accounts partially for changes in linewidth and intensity. These classical molecular dynamics simulations also elucidate the behavior of the isotropic Raman spectrum in the bulk liquid upon isotopic dilution. We also simulate the resonant coupling among cyano stretches in this system. These simulations match the experimental shift due to the Raman non-coincidence effect shift of the CN stretch in the bulk liquid, but suggest that the corresponding resonant-coupling-induced shift in the VSFG spectrum at the silica interface is minimal. Our experimental and simulation results indicate that proximity to an interface can cause substantial changes in the resonant coupling of vibrations in a liquid.

2

1. Introduction

Vibrational sum-frequency generation (VSFG) spectroscopy is a powerful and widely used technique for studying molecular orientation and organization at interfaces [1-6]. This technique relies on the overlap of an infrared (IR) laser beam and a visible or near-infrared laser beam at an interface, which can generate a signal with a frequency that is equal to the sum of the frequencies of the two incident beams. When the energy of the IR beam is coincident with a dipole-allowed vibrational transition, the signal becomes resonantly enhanced. As a second-order nonlinear optical technique, VSFG is forbidden in centrosymmetric media under the electric dipole approximation [7]. However, a signal can be generated at the interface between two isotropic media, where centrosymmetry is necessarily broken. Therefore, VSFG measurements are sensitive to regions with thicknesses as small as one to a few molecular layers, avoiding the contribution of the far more numerous bulk molecules. Detailed insights into the molecular organization at an interface can often be gained by using different polarization combinations of the input and signal beams [4, 8-11].

VSFG spectra are generally interpreted within a static picture, and in terms of the spectroscopic properties of individual molecules. There is a growing recognition, however, that dynamics can play an important role in VSFG spectra [6]. In condensed-phase systems, dynamic processes such as reorientation and energy transfer can occur on a time scale of picoseconds or less [6]. This time scale is comparable to that of the lifetimes of the vibrational coherences that are probed in VSFG spectroscopy. Thus, such dynamic processes can act as dephasing mechanisms that influence the intensity and shape of peaks in VSFG spectra. In the case of reorientation, the sensitivity of a VSFG measurement depends on the polarization configuration, the symmetry of the vibrational modes being probed, and, in implementations using ultrafast

3

lasers, the timing delay between the incident IR and probe pulses [6, 12-15]. Furthermore, reorientation can cause the same oscillator to encounter different dielectric environments on a time scale that is shorter than the vibrational coherence time, inducing a time dependence to the vibrational frequency. This phenomenon, which is called reorientation-induced spectral diffusion (RISD), can influence VSFG spectra of vibrational modes, including modes that would not otherwise be sensitive to reorientation [16].

Intermolecular vibrational coupling via transition-dipole/transition-dipole and other interactions also has the potential to play a role in VSFG spectra [17]. The coupling strength, J, between two transition dipoles μ_1 and μ_2 that are separated by distance r is given by

$$J = \frac{\mu_1 \mu_2}{4\pi\varepsilon_0 r^3},$$
(1)

where ε_0 is the vacuum permittivity. We note that this expression for the coupling magnitude ignores orientational effects, which are discussed below. There are two limiting cases of resonant vibrational coupling, which are distinguished by the strength of the coupling relative to the vibrational linewidth, Γ. Förster transfer occurs when $J \ll \Gamma$, allowing an excitation to hop among oscillators. Efficient Förster transfer in the bulk generally requires molecules with functional groups that have large dipole moments and large transition-dipole moments, but this condition may be less important at an interface, because geometrical effects can govern the proximity of vibrational transition dipoles on neighboring molecules. Several groups have employed time-resolved VSFG spectroscopy to help shed light on vibrational Förster transfer at interfaces. Such experiments have made it possible to infer the time scale of energy transfer [18], to distinguish energy transfer from other processes through isotopic dilution [19], and to probe the surface coverage of monolayers on single crystal surfaces [20]. Because OH groups have

4

large transition dipoles, water exhibits intermolecular vibrational coupling that needs to be considered in the analysis of VSFG studies of this liquid [21-23]. Energy transfer between oscillators on the same molecule may also play a role in the VSFG spectroscopy of larger species [19, 24].

When J becomes comparable to Γ, energy transfer occurs on the time scale of other mechanisms of vibrational dephasing [6, 20]. In this limit, the coupling is better described in terms of a vibrational exciton, in which the excitation is delocalized coherently over multiple molecules. This distinction between the two limiting cases has important implications for VSFG spectra. For example, Förster energy transfer causes dephasing and line broadening in a manner similar to that of reorientation. As is the case for reorientation, Förster energy transfer has a greater influence on spectra of depolarized vibrational modes than on spectra of isotropic vibrational modes [6]. On the other hand, excitonic coupling preserves vibrational coherence, but can influence VSFG spectra because the coherence is spread over many molecules. This phenomenon can affect VSFG measurements [6, 22, 23], but may also be mistaken for other dynamic processes, such as reorientation.

The influence of resonant coupling on VSFG spectra is only beginning to be explored. Heterodyne-detected VSFG studies of the liquid water/vapor and ice/vapor interfaces [22, 23] revealed a red shift and broadening of the O-H stretch that is associated with near-resonant coupling. These spectral changes mirror those in the bulk, but are less pronounced near an interface, where molecules have fewer nearest neighbors [23]. Carbon monoxide adsorbed to ruthenium is also presumed to exhibit excitonic coupling at high enough surface coverages [20].

In some of these situations, the J values alone may not seem large enough to suggest the presence of excitonic coupling. At an interface, however, other structural factors must be

considered. For instance, when the distance between dipoles is closer than the distance between charge separation on the individual dipoles, coupling may be stronger than expected from a simple multipole model [25]. Also, coupling may extend over many nearest neighbors at a well-organized interface.

Another important aspect of transition-dipole coupling is that the spectroscopic manifestation of this phenomenon depends on the manner in which a vibrational transition is probed [26-28]. Different excitation mechanisms lead to different effective pairwise transition-dipole interactions, which is the essence of the Raman non-coincidence effect (RNCE), in which the spectral position of the isotropic Raman peak of a mode differs from the position of the same mode's depolarized Raman peak. If the mode is also infrared active, the position of the corresponding IR absorption peak may be different from those of the isotropic and depolarized Raman peaks.

The liquid acetonitrile/silica interface is a useful model system for exploring the processes that influence VSFG spectra [6]. Acetonitrile is a relatively simple, amphiphilic molecule. Liquid acetonitrile undergoes strong ordering at silica surfaces, as has been studied extensively with both simulations [29-34] and experiments [30, 34, 35]. In the bulk, acetonitrile is thought to dipole-pair to some extent [36], although there is now evidence the antiparallel molecules take on more of an "octupole-paired" structure [37, 38]. Evidence exists for a degree of resonant coupling of the cyano stretch of acetonitrile in the bulk, leading to shifts among its isotropic and anisotropic Raman spectra and its IR spectrum [26, 39], but a smaller shift might be expected for the symmetric methyl stretch, as the methyl group has a smaller permanent dipole moment [40]. At a silica interface, on the other hand, acetonitrile forms a supported lipid-bilayer-like (LBL)

structure [41]. Methyl groups form the hydrophobic interior of the layer, and so their vibrations may have the opportunity to interact more strongly than in the bulk liquid.

Isotopic dilution is a classic means of determining the importance of the RNCE for specific vibrational modes, as this type of dilution decreases the degree of vibrational coupling without changing the physical properties of the liquid substantially. Here we use VSFG spectroscopy to examine the transition frequency of the acetonitrile methyl symmetric stretch at the acetonitrile/silica interface in mixtures with acetonitrile-d_3 over a broad range of concentrations. The dependence of the spectrum on the acetonitrile mole fraction cannot be described fully in terms of the properties of individual acetonitrile molecules. Through a combination of experiments and molecular simulations, we find that resonant coupling is a significant driver of the concentration dependence of the transition frequency for the symmetric methyl stretch of acetonitrile at this interface in VSFG spectra, but is not the dominant effect. Nevertheless, resonant coupling leads to a larger shift in the infrared band for the symmetric methyl stretch at the silica interface than in the bulk. Our simulations also provide an explanation for the behavior of the isotropic Raman spectrum of bulk liquid acetonitrile upon isotopic dilution. Additionally, these simulations indicate that for the cyano stretch of acetonitrile at the silica/liquid interface, the resonant coupling is smaller than in the bulk.

2. Experimental and computational methods

VSFG experiments were performed with a counterpropagating setup that has been described in detail elsewhere [16, 42]. Briefly, a 1 kHz Ti-Sapphire regenerative amplifier (Legend Elite, Coherent) produces 3 W of 800 nm, 80 fs pulses. The amplifier is seeded with the output of a Ti:Sapphire laser (Mira, Coherent), which passes through a MIIPS pulse shaper [43] to ensure that the 800 nm probe pulse is transform-limited at the sample. 1 W of the amplified beam is sent

into an optical parametric oscillator/difference-frequency generation module (TOPAS, Light Conversion), which generates 15 mW of output centered at 2940 cm^{-1} with a bandwidth of 250 cm^{-1}. Another 1 W of the amplifier output is sent through a slit in a $4f$ pulse stretcher to produce 15 mW of 800 nm probe light with a bandwidth of 5 cm^{-1}. The incident IR and probe beams are directed onto the sample at angles of -58° and 61°, respectively, from the surface normal, and the signal emerges, according to the phase-matching conditions, at -32.8°. The signal is collected using a spectrometer (ActonSP300i) with a thermoelectrically-cooled CCD camera (Spec-10:100, Roper Scientific). All experiments were performed at room temperature (295 K).

The chemicals used for the isotopically diluted acetonitrile solutions were 99+% spectroscopic grade acetonitrile (ACROS) and 99.5% (D-99.8%) acetonitrile-d_3 (Cambridge Isotope Laboratories). Concentrations ranging from 0.05 to 1 mole fraction of acetonitrile in acetonitrile-d_3 were used. All sample cuvettes were IR-grade quartz with a 1-mm pathlength (Hellma). Prior to use, the cuvettes were rinsed with contaminant-free [44] acetone, methanol, and then water. The cuvettes were subsequently oven-dried, and then cleaned for 3 min in an oxygen plasma. Each sample was added to a clean cuvette, rather than performing subsequent dilutions in the same cuvette, to avoid having any vestiges of the higher-concentration mixtures remain behind, potentially influencing the subsequent measurement. Spectra were collected in the *SSP* polarization configuration, with the polarizations listed in the order of the signal, probe, and IR beams. *P* indicates a polarization parallel to the plane of incidence, and *S* indicates a polarization perpendicular to this plane. Three 60 s scans were performed at high acetonitrile mole fractions, and six 120 s scans were performed for mole fractions of 0.1 and lower. All spectra were normalized to the nonresonant SFG signal of a gold substrate and were frequency

calibrated using four absorption peaks of a polystyrene film placed in the path of the IR beam while measuring the gold SFG signal.

Molecular dynamics simulations were performed using a 6-site, all-atom, flexible model for acetonitrile that reproduces both experimental structural and dynamic properties of the bulk liquid [45] and the behavior of the liquid at silica interfaces [29]. For the non-bonded component, the sites interact through a pair potential consisting of the sum of a 12-6 Lennard-Jones potential and a Coulombic term:

$$E_{non-bonded} = \sum_i \sum_{j \neq i} \left\{ 4\varepsilon_{ij} \left[\left(\frac{\sigma_{ij}}{r_{ij}} \right)^{12} - \left(\frac{\sigma_{ij}}{r_{ij}} \right)^6 \right] + \frac{1}{4\pi\varepsilon_0} \frac{q_i q_j}{r_{ij}} \right\}, \tag{2}$$

where i and j are the different sites, ε_{ij} and σ_{ij} are the Lennard-Jones well depth and site radius, respectively, r_{ij} is the separation distance between sites i and j, and q_i and q_j are the charges on sites i and j, respectively. For atoms on the same molecule, the 1,4 electrostatic interactions are scaled by a factor of 0.83, and the 1,4 Lennard-Jones interactions are scaled by a factor of 0.5. There is also a bonded component with harmonic bond and angular bending terms given by

$$E_{bonded} = \sum_{bonds} K_r (r - r_0)^2 + \sum_{angles} K_\theta (\theta - \theta_0)^2, \tag{3}$$

where K_r is the harmonic bond coefficient, r_0 is the equilibrium value of the bond distance r, K_θ is the harmonic angular coefficient, and θ_0 is the equilibrium value of the angle given by θ.

All molecular dynamics simulations were performed using the LAMMPS package [46] with the potential in Eqs. (2) and (3) for acetonitrile. The equations of motion were integrated every 1 fs using the Verlet algorithm. For the acetonitrile/silica simulations, all silicon and oxygen atoms were fixed. The interfacial OH groups could rotate freely. The length of the O−H bond was constrained using the SHAKE algorithm [47] to be 1.0 Å. The Si−O−H angular bending

potential had an equilibrium value of 109.27° with a bending strength of 200.0 kcal/mol. The hydroxylated silica surface had partial charges on the silanol groups, following previous work [48], with the charges on the bulk silicon and oxygen atoms set to zero. For the acetonitrile/silica simulations, the interaction between acetonitrile and silica consisted of a 12-6 Lennard-Jones component and a Coulombic component, as in Eq. (2). The interaction cutoff lengths for both the Lennard-Jones and Coulombic interactions in all simulations were set to 14 Å, with standard Lorentz-Berthelot combining rules used for the Lennard-Jones interactions. Long-range Coulombic interactions in the bulk simulations were calculated using Ewald summation, which was optimized by LAMMPS. Periodic boundary conditions were used in all three dimensions for the bulk acetonitrile simulations. In the acetonitrile/silica simulations, a particle-particle-particle-mesh solver with a slab geometry (periodic in the x and y dimensions, non-periodic in the z dimension) was used, with a tolerance of 10^{-5}.

For the bulk simulations, an initial configuration consisting of 529 acetonitrile molecules was built using PACKMOL [49], and an energy minimization was performed with a tolerance of 10^{-6}. The system was then equilibrated for 200 ps in the *NPT* ensemble at a pressure of 1 bar and a temperature of 298 K. A Nosé-Hoover thermostat and barostat [50, 51] were used, with relaxation constants of 30 and 1000 fs, respectively. A production run of 2 ns in the *NPT* ensemble was then performed to find the equilibrium density of acetonitrile, which was within 1% of the literature value for the force field [45]. Using the determined density, an initial configuration of 524 acetonitrile molecules in a 36 Å × 36 Å × 36 Å box was built using PACKMOL, an energy minimization was performed with the same tolerance as before, and the system was equilibrated in the *NVT* ensemble with a temperature of 298 K and a Nosé-Hoover thermostat with a relaxation constant of 30 fs. After equilibration, a production run was

performed for 2 ns in the *NVE* ensemble. The entire trajectory was analyzed using configurations spaced by 1 ps to calculate the angularly-resolved radial distribution functions and by 10 ps to calculate the spectral shifts, in accordance with the integrated correlation times.

For the acetonitrile/silica simulations, a crystalline silica substrate was used with the oxygen atoms in the silanol forming a close-packed FCC (111) structure and the surface density of 4.5 hydroxyl groups per nm^2, following previous work [29, 52]. The in-plane dimensions were $L_x = 40.5368$ Å and $L_y = 35.1059$ Å. A hydrophobic wall with a potential consisting of the repulsive part of a 12-6 Lennard-Jones potential [53] was located at a z distance of 100.0 Å from the plane of the silanol silicon atoms, so that adsorption would occur only on one side of the silica surface. Beyond the hydrophobic wall, vacuum was implemented for 50.0 Å in the z direction to ensure the correct calculation of the long-range interactions. Fixed boundary conditions were used in the z dimension. An initial configuration of acetonitrile was built using PACKMOL [49]. The configuration included 864 molecules confined in the z dimension between the silica substrate and the hydrophobic wall. An energy minimization was first performed with an energy tolerance of 10^{-6}. A simulation was then performed for 1 ns in the *NVT* ensemble at a temperature of 348 K to equilibrate the system, followed by a simulation for 200 ps in the *NVT* ensemble at a temperature of 298 K. The same Nosé-Hoover thermostat and relaxation constant were used as in the bulk simulations. A production run of 40 ns in the *NVT* ensemble was performed to obtain sufficient statistics for the density profiles. Configurations were saved every 1 ps. The entire trajectory was analyzed to calculate density profiles and potential heat maps. As with the data for the bulk system, the entire trajectory was analyzed using configurations spaced every 1 ps to calculate angularly-resolved radial distribution functions. Configurations were analyzed every 100 ps to calculate spectral shifts, in accordance

with the integrated correlation times. In the calculation of time-correlation functions of the frequency shift in either of the interfacial sublayers, time points at which a given molecule was not within the chosen sublayer were not considered. Based on the charges on the atoms in the methyl group, the position of the methyl stretch transition dipole was taken to be 1.481 Å from the center of mass along the molecular axis. For the cyano group, the position of the transition dipole was taken to be along the molecular axis, equidistant from both atoms.

Angularly-resolved radial distribution functions, $g(r,\theta)$ were calculated, including the cone correction, by integrating in spherical coordinates over both the distance r and the angle θ between transition dipoles (the latter of which was determined from the angle between the principal axes of the molecules) [37]. The angularly-resolved radial distribution function gives orientational information that is not accessible from the radial distribution function, $g(r)$, which is averaged over all angles.

To explore the influence of isotopic dilution on resonant coupling, we used the same molecular dynamics trajectories. A uniform pseudorandom number generator was used to select acetonitrile molecules to tag as "deuterated" throughout the entire trajectory. These molecules were not considered in the analysis of resonant coupling. Other effects, such as the slight changes in molecular volume and viscosity between acetonitrile and acetonitrile-d_3, were not considered in this analysis.

3. Results and discussion

The effect of isotopic dilution on the *SSP* VSFG spectrum of the methyl stretching region of liquid acetonitrile at the silica interface is shown in Fig. 1A. Spectra in this region consist of a peak at ~2943 cm^{-1} that corresponds to the symmetric methyl stretch. The strong signal indicates

that the molecular axis has a large projection along the surface normal, given that Raman transition for the methyl symmetric stretch is highly polarized, i.e., this transition is dominated by the isotropic portion of the Raman tensor (*vide infra*). The slight asymmetry is consistent with previously published results, and is believed to arise from the contribution of two oppositely phased peaks, with slightly different center frequencies and amplitudes, that correspond to the contributions from the two different sublayers of the LBL structure [16, 30, 34, 54, 55]. Upon dilution with acetonitrile-d_3, the spectrum exhibits a blue shift and narrows, as can be seen in the normalized spectra in Fig. 1B. The spectra also become slightly more asymmetric upon dilution. We note that no signal was observed in this spectral region in the neat acetonitrile-d_3.

If the organization of the liquid remains unchanged upon isotopic dilution, then the VSFG intensity would be expected to scale with the square of the number of oscillators. Such behavior has been observed previously at the liquid/vapor interface of acetonitrile/acetonitrile-d_3 mixtures [56], which indicates that isotopic dilution does not affect the organization of acetonitrile at that interface. In contrast, as shown in Fig. 2A, upon isotopic dilution the intensity at the acetonitrile/silica interface becomes larger than predicted by this model. Although the excess intensity is modest, it is clear from Fig. 2B that there is a systematic trend in which the ratio of the observed intensity to the expected intensity grows with increasing acetonitrile-d_3 mole fraction.
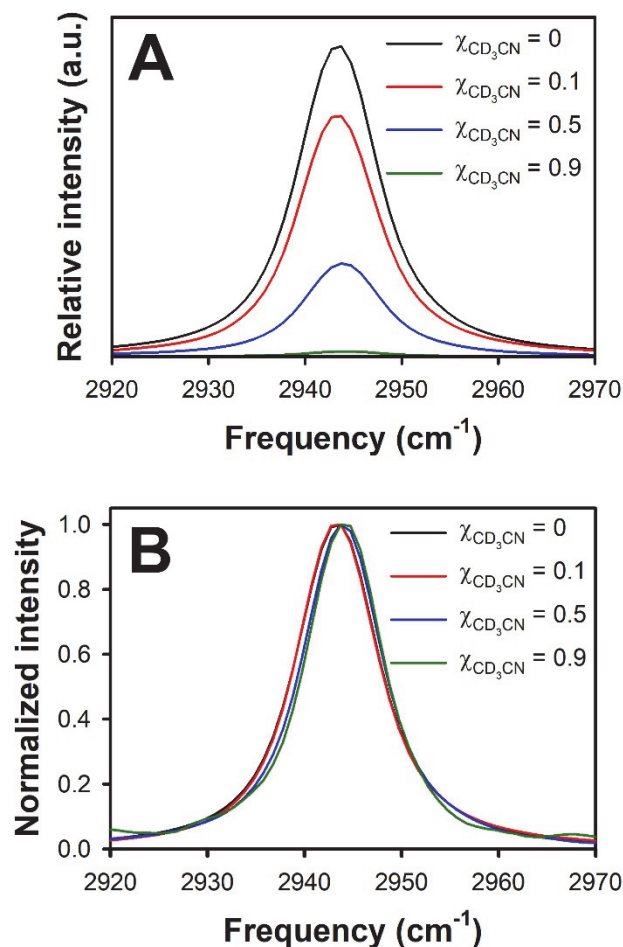
Fig. 1. (A) Experimental VSFG spectra of liquid acetonitrile/acetonitrile-d_3 mixtures at a silica interface obtained under *SSP* polarization conditions in the methyl-stretching spectral region. (B) Normalized spectra emphasize the blue shift, narrowing, and slight increase in asymmetry at low acetonitrile mole fractions.

The results from the liquid/vapor interface [56] suggest that the organization at the silica/liquid interface should not change upon isotopic dilution. Because hydrogen bonds from surface silanols are accepted by the cyano groups, it is also unlikely that isotopic substitution of the methyl group influences partitioning to the silica surface. At the temperature at which our

experiments were performed, the viscosity of acetonitrile-d_3 (0.382 cP) is ~9% larger than that of acetonitrile (0.350 cP) [57], which will lead to somewhat slower orientational dynamics with increasing acetonitrile-d_3 mole fraction. However, this viscosity change is modest, and reorientation has a minimal influence on the symmetric methyl stretch spectrum at this interface [58], so orientational dynamics cannot play a major direct role in the observed behavior. As we shall see below, however, these dynamics can play an indirect role. Furthermore, an increase in viscosity would also be expected to decrease the influence of RISD in the second sublayer of acetonitrile, which would decrease the VSFG intensity. Thus, we must search for another explanation for this intensity anomaly.

The spectral shift and line narrowing observed with increasing acetonitrile-d_3 mole fraction are quantified in Figs. 3A and 3B, respectively. We note that although our probe bandwidth is 5 cm^{-1}, because the spectrum of acetonitrile features only a single peak we can determine the peak position to within a small fraction of a wavenumber. The overall spectral shift in going from pure acetonitrile to infinite dilution is 1.3 cm^{-1}, and the total decrease in the full width at half maximum (FWHM) is 0.7 cm^{-1} (7% of the FWHM in the neat liquid). Before considering the meaning of these observations, we first review what has been observed in the vibrational spectroscopy of the bulk isotopic mixtures of this liquid.
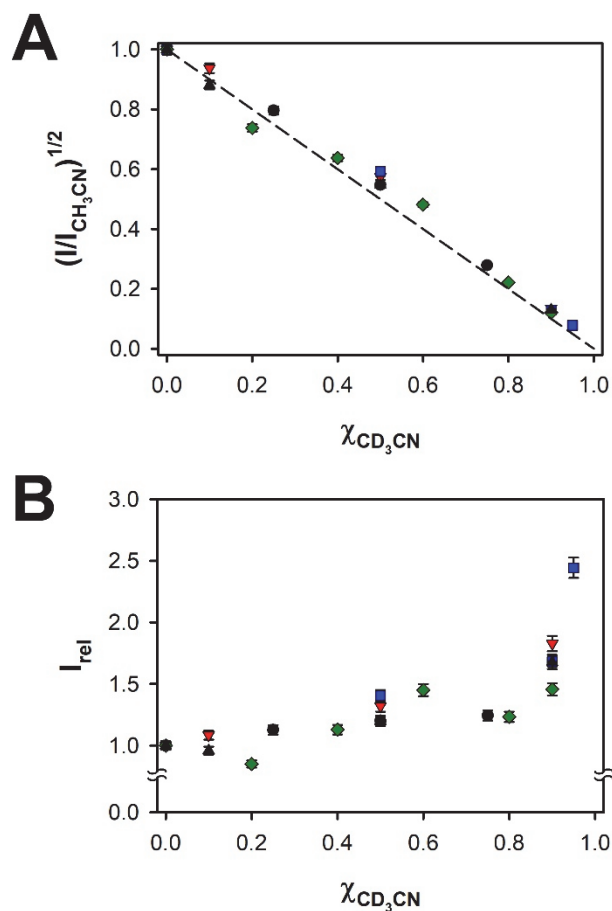
Fig. 2. (A) The square root of the intensity, relative to that of the neat liquid, of the symmetric methyl stretch peak in *SSP* VSFG spectra of liquid acetonitrile at the silica interface as a function of mole fraction of acetonitrile-d_3. The dashed line is the result expected if the interfacial concentration mirrors that in the bulk and no collective spectroscopic effects are considered. (B) The ratio of the observed intensity to the expected intensity. The different colors denote data obtained on different days. The error bars represent the variation in the measurement of a specific sample, including the uncertainty in normalization.
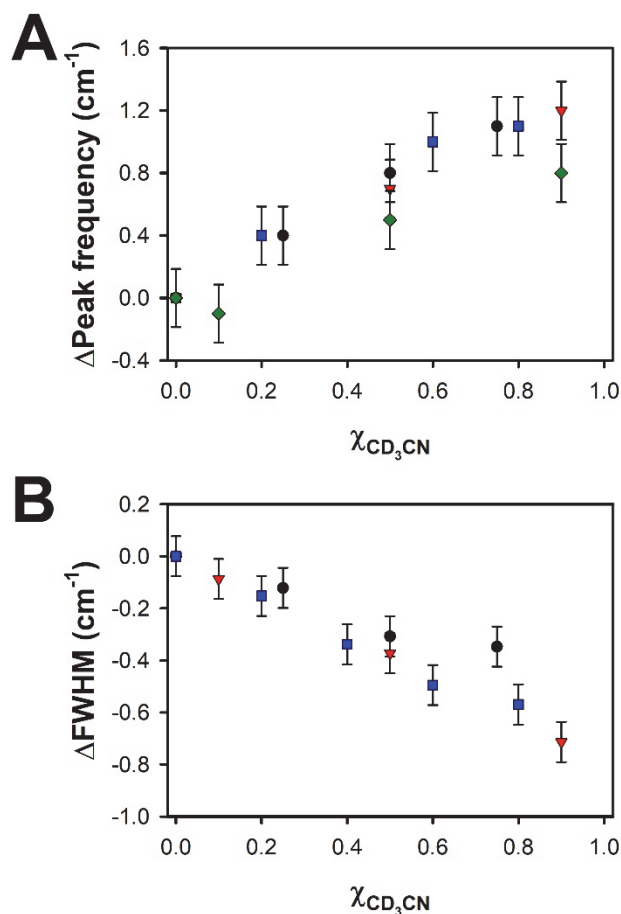
Fig. 3. Dependence of (A) the peak frequency and (B) the linewidth of the symmetric methyl stretch peak in the VSFG spectrum of liquid acetonitrile at the silica interface as a function of the mole fraction of acetonitrile-d_3. The different colors denote data obtained on different days.

Isotropic Raman difference spectroscopy studies of the influence of isotopic dilution on the symmetric methyl stretch of bulk acetonitrile have revealed a blue shift that is linear with concentration and reaches a value of 1.8 cm^{-1} at infinite dilution [59-61]. Isotropic Raman experiments performed on the bulk liquid indicate that the linewidth of the symmetric methyl stretch (6.0 cm^{-1}) does not change appreciably upon isotopic dilution [62, 63]. At a 50% isotopic dilution, the IR linewidth for the symmetric methyl stretch has been observed to narrow slightly

(from 13.4 cm^{-1} in the neat liquid to 13.1 cm^{-1}) and the depolarized Raman linewidth has been observed to decrease somewhat more substantially (from 14.0 cm^{-1} in the neat liquid to 12.2 cm^{-1}) [63].

The behavior of the isotropic Raman spectrum upon isotopic dilution was attributed by Asthana *et al*. to inhomogeneities in the local dielectric environment [59], as described by the model of Knapp and Fischer [64]. However, Raman echo experiments performed on the symmetric methyl stretch of pure acetonitrile detected no inhomogeneous broadening in the isotropic Raman spectrum of this mode [65]. A simple model of the extent of inhomogeneous broadening based on the spectral properties in the neat liquid and at infinite dilution supports this picture [66]. Furthermore, the significantly narrower linewidth in the isotropic Raman spectrum indicates that reorientation plays a substantial role in the IR and depolarized Raman spectra, and the narrowing of these latter spectra upon dilution may, in part, be the result of the abovementioned increase in viscosity [57]. Thus, it is doubtful that such a picture can account for the observed concentration dependences of the center frequency and linewidth of the isotropic Raman spectrum in this system.

Marri *et al*. observed no change in the vibrational dephasing rate in the isotropic Raman spectrum of the symmetric methyl stretch of acetonitrile upon isotopic dilution [62]. This observation is consistent with this transition having minimal inhomogeneous broadening. These authors suggested that the behavior of this transition upon isotopic dilution can be understood via Kubo theory, including a combination of an attractive, dipole contribution, which would lead to a red shift, and a repulsive contribution, which would lead to a blue shift [62]. Ben-Amotz *et al*. studied the Raman spectrum of this mode upon dilution in a number of different solvents, finding a red shift, or no shift at all, in each case [67]. This latter work also indicated that attractive

forces beyond dipole/dipole interactions, such as those involving polarizability, play a role in the transition frequency. Given that the dipole moments and refractive indices of acetonitrile and acetonitrile-d_3 are virtually identical, the attractive interactions of the two species are likely to be nearly identical as well. Because the isotropic Raman spectrum shifts to the blue upon isotopic dilution, within this picture repulsive interactions must dominate the shift. The molar volumes of the two liquids are also virtually identical [68, 69], which suggests that density effects do not contribute to the blue shift in the isotropic Raman peak upon isotopic dilution. As noted above, the viscosity of acetonitrile-d_3 is ~9% larger than that of acetonitrile at the temperature at which our experiments were performed. The increased caging in acetonitrile-d_3 could therefore plausibly contribute to the observed blue shift upon isotopic dilution.

Kamogawa and Kitagawa attributed the behavior of the isotropic Raman spectrum of acetonitrile with isotopic dilution to resonant coupling [61], although the fact that Marri *et al*. did not find a measurable change in the dephasing rate of this mode upon isotopic dilution [62] conflicts with this conclusion. There is precedent for strong excitonic coupling of molecular vibrations in liquids, such as benzene, for example [70]. Coupling of symmetric methyl stretches would not be expected to be particularly strong in general, but acetonitrile is a small enough molecule that the density of methyl groups is high. To evaluate the importance of resonant coupling of the methyl symmetric stretch in this liquid, it is necessary to consider whether the magnitude of J in Eq. (1) could be large enough to be in the excitonic regime. The magnitude of J depends upon the value of the transition-dipole moment for the symmetric methyl stretch. We could not find a literature value for the transition dipole of the symmetric methyl stretch of acetonitrile, and values for the same mode in other molecules span a large range. Andrews and Boxer give a value of 0.061 D for the symmetric methyl stretch in acetonitrile-d_3 [40], which can

be regarded as a lower bound, as deuteration should decrease the dipole moment somewhat. To determine an upper bound for the observed shift in the bulk isotropic Raman spectrum based on our simulations (*vide infra*), under the assumption that the entire shift arises from resonant coupling, we use a value of 0.013 D^2 for the square of the transition dipole. This value is within the range of those previously reported [71-74]. Given this value, we find that

$$J \cong \frac{130 \text{ cm}^{-1}\text{Å}^3}{r^3} \,, \tag{4}$$

where r is in units of Ångstroms. We will use this upper limit as a starting point. As the coupling scales with the square of the transition-dipole moment, in the lower limit J is a factor of ~3.5 smaller.

For the silica/liquid interface, the linewidth of our VSFG spectra is on the order of 10 cm^{-1}, but accounting for our spectroscopic resolution and the presence of two opposing spectral features, the homogeneous linewidth is more likely on the order of 5 cm^{-1}. Ignoring orientational effects, the resonant coupling is expected to be in the excitonic regime for distances short enough that $J \geq \Gamma$. The largest separation for which $J \geq 5$ cm^{-1} is on the order of 2.4 Å. Thus, in this picture, acetonitrile could be near to the vibrational exciton regime for the symmetric methyl stretch in the bulk liquid, and, as we shall see below, even more so at the silica/liquid interface. Of course, if the transition dipole squared is closer to the lower limit, this picture will change.
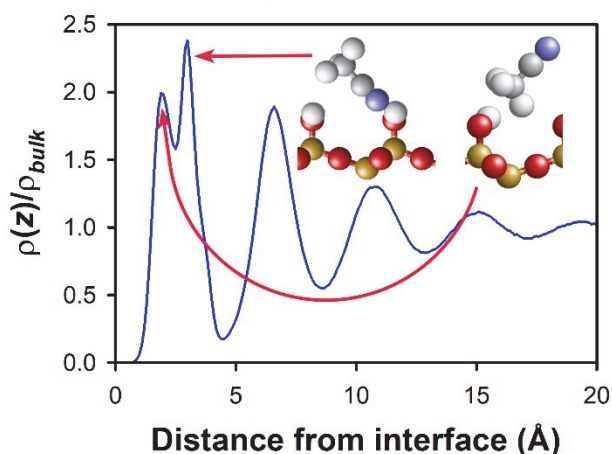
Fig. 4. Local density of acetonitrile methyl transition dipoles, normalized to the bulk density, as a function of distance from the interface. The z coordinate of the plane of the oxygen atoms in the silanol groups is used as the position of the interface ($z = 0$), following previous work [29]. Also shown are representative molecules in the first sublayer (the second density peak) and the second sublayer (the first density peak).

Shown in Fig. 4 is the density of methyl transition dipoles as a function of distance from the silica surface, as determined from our simulations. This distribution has several features that are relevant to understanding resonant energy transfer of the methyl symmetric stretches of the interfacial molecules. The first peak in the distribution, at ~1.9 Å from the silica surface, corresponds to molecules in the second sublayer that have methyl groups that point roughly toward the silica surface. The density of these methyl transition dipoles is considerably greater than that in the bulk liquid, which could promote enhanced resonant coupling. The second peak, at ~3.0 Å` from the silica surface, arises from the methyl transition dipoles of the molecules in the first sublayer. The density of these methyl transition dipoles is even greater than that in the first peak, because the first sublayer is more strongly ordered. The shoulder of the second peak,

at ~4.5 Å, arises from molecules in the second sublayer that have methyl groups that point roughly into the bulk liquid. For comparison, density profiles for the nitrogen atom and the methyl carbon atom are given in the supporting information (Figs. S1A and S1B, respectively), and are in good agreement with the work of Hu and Weeks.[29]

The density of methyl transition dipoles reaches a local minimum of approximately 1/6 of the bulk methyl transition dipole density at a distance of ~4.8 Å from the silica surface. The next maximum is at a distance of ~6.6 Å from the silica surface. The deep density minimum and the relatively large distance of the third density peak from the first two density peaks largely decouple the methyl transition dipoles in the surface bilayer from rest of the liquid. Furthermore, the difference in the methyl symmetric stretch frequency between the first and second sublayers reduces interlayer resonant coupling. Thus, to a first approximation we might expect to have separate vibrational excitons for the methyl symmetric stretch in the first and second sublayers, with only mild intermixing.

Fig. 5A is a plot of the angularly-resolved radial distribution function [37] for the methyl symmetric stretch transition dipole for the surface bilayer, and Fig. 5B is a corresponding plot for the bulk liquid. A difference map between the two distributions is shown in Fig. 5C. Representative pair configurations from different regions of the difference map are shown in Fig. 5D. The radial distribution functions $g(r)$ are broad and relatively featureless both in the bulk liquid and at the interface. The difference map highlights the angles and distances that are favored in the bulk liquid over the interface (violet through green in the heat map, in order of increasing difference) and that are favored at the interface over the bulk liquid (yellow through red in the heat map, in order of increasing difference). The two structural motifs that have the greatest prevalence in the bulk liquid rather than at the interface are perpendicular neighbors with

the cyano group of one molecule near the methyl group of another molecule (representative pair 1) and with the two methyl groups near to one another (representative pair 2). On the other hand, parallel neighbors (representative pairs 3 and 4) and antiparallel neighbors (representative pairs 5 and 6) are considerably more likely to be found at the interface than in the bulk liquid. We stress that configurations shown in Fig. 5D are not necessarily the ones most commonly found in the bulk or at the interface, but rather the ones that are most likely to be found in one environment but not the other.
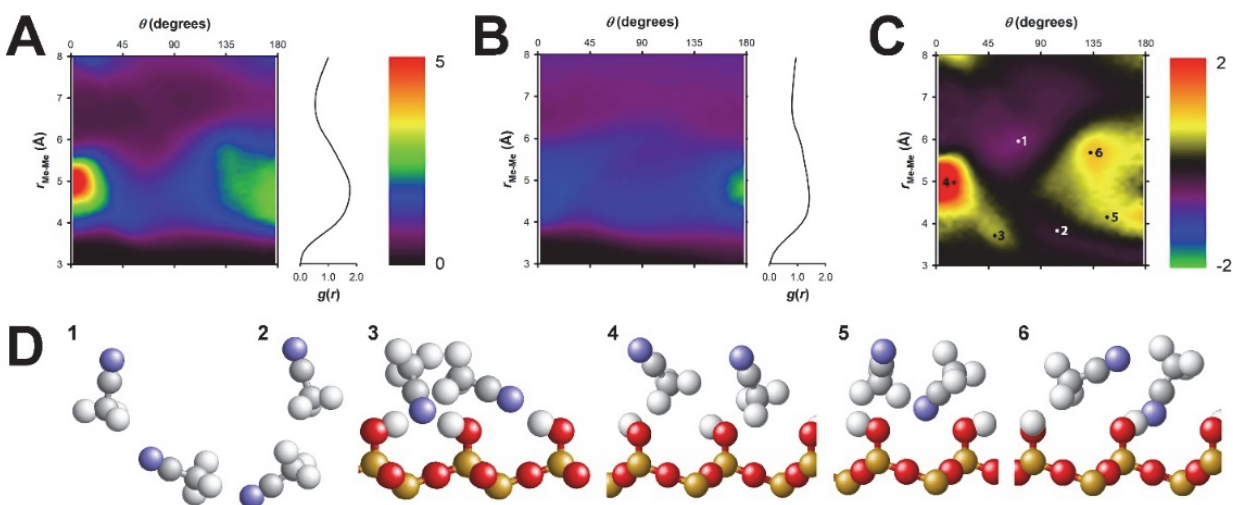

Fig. 5. Angularly-resolved radial distribution functions and radial distribution functions for the methyl transition dipole in (A) the surface bilayer of acetonitrile at a silica interface and (B) bulk liquid acetonitrile. (C) A difference map between the angularly-resolved radial distribution functions for the interfacial bilayer and the bulk liquid, and (D) the representative pair configurations denoted in (C), including surface silanol groups for the interfacial pairs. The atoms shown are nitrogen (blue), carbon (gray), hydrogen (white), oxygen (red) and silicon (gold). The color scale is the same in (A) and (B).

The frequency and width of the methyl symmetric stretch peak of acetonitrile at the silica interface may differ from those in the bulk liquid for a number of reasons, including the higher density of the interfacial bilayer. For this reason, we will focus on the relative trends of the frequency and width upon isotopic dilution in these different environments. From a resonant coupling perspective, the interaction potential between two molecules i and j depends on the distance between and strength of the transition-dipole moments, and the relative orientation of neighboring transition dipoles via [26]

$$V_{ij}^{(2)} = \frac{\mu^2}{r^3}\left[\mathbf{n}_i \cdot \mathbf{n}_j - 3(\mathbf{n}_i \cdot \mathbf{n})(\mathbf{n}_j \cdot \mathbf{n})\right] \; , \tag{5}$$

where $\mathbf{n_k}$ is a unit vector along the transition dipole of molecule k, and $\mathbf{n}$ is the unit vector between transition dipole i and transition dipole j.

The shift in the isotropic spectrum due to resonant coupling is calculated by averaging Eq. (5) over this distribution of transition dipoles

$$\Delta\tilde{\nu}_{iso} = \frac{2}{N}\sum_{i<j}^{N} \langle V_{ij}^{(2)} P_0(\cos\theta_{ij})\rangle \, , \tag{6}$$

where N is the number of molecules, θ_{ij} is the angle between molecules i and j, and P_0 is the zero-order Legendre polynomial. We note that this equation is sometimes given in the literature with a prefactor of $1/Nm\omega_0$, but Eq. (6) is correct when the transition dipole, rather than the dipole derivative with respect to the vibrational coordinate, is used. The corresponding shifts for the IR spectrum and the depolarized Raman spectrum are

$$\Delta\tilde{\nu}_{IR} = \frac{2}{N}\sum_{i<j}^{N} \langle V_{ij}^{(2)} P_1(\cos\theta_{ij})\rangle \, , \tag{7}$$

and

$$\Delta\tilde{v}_{dep} = \frac{2}{N}\sum_{i<j}^{N}\langle V_{ij}^{(2)}P_2(\cos\theta_{ij})\rangle,\qquad(8)$$

respectively.

The angularly-resolved radial distribution function for the bulk liquid shows that the angles between the transition dipoles for the symmetric methyl stretch corresponding to the first peak in $g(r)$ are relatively evenly distributed, with a small peak in the region of ~170° to 180°. The angularly-resolved radial distribution function for the surface bilayer shows that there is a significant probability of finding methyl transition dipoles on neighboring molecules making angles that are less than 45° and greater than 135°. The probability distribution is therefore skewed towards parallel and antiparallel molecules, as would be expected given the supported LBL organization at the interface. To determine the spectroscopic implications of the angularly-resolved radial distribution function for the interfacial molecules, it is useful first to consider some aspects of the VSFG signal. In VSFG spectroscopy, the IR pump beam creates a vibrational coherence at time 0 that is probed time t later via a Raman transition. The Raman transition can be decomposed into an isotropic component and a depolarized component [75]. For the symmetric methyl stretch, both the isotropic and depolarized portions of the Raman tensor contribute to the VSFG response function under *SSP* polarization conditions, via [6]

$$R_{xxz} \propto \mu'\alpha_I'\langle\cos(\theta)\rangle + \mu'\alpha_A'\left(\frac{1}{12}\langle\cos(\theta)\rangle + \frac{1}{4}\langle\cos(\theta)\cos(2\Theta)\rangle\right),\qquad(9)$$

where μ', α_I', and α_A' are the derivatives with respect to the symmetric methyl stretch coordinate of the dipole moment, the isotropic component of the polarizability, and the anisotropic component of the polarizability, respectively, θ is the angle that the transition dipole makes with the surface normal at the time of the IR transition, and Θ is the angle that the transition dipole makes with the surface normal at the time of the Raman transition. For the symmetric methyl stretch of

acetonitrile, α_I', is more than 3 times greater than α_A' [11, 58, 76]. Thus, Eq. (9) indicates that under

SSP polarization conditions, the VSFG signal for the symmetric methyl stretch in acetonitrile is

dominated by the isotropic portion of the polarizability, and therefore the strong *SSP* signal reflects

a significant average projection of the transition dipole along the surface normal. But what

influences the shift due to resonant coupling in a VFSG spectrum: the isotropic portion of the

polarizability, the depolarized portion of the polarizability, the IR transition dipole, or some

combination of the three? To our knowledge, this issue has not been addressed previously in the

VSFG literature.

The Legendre polynomials in Eqs. (6) – (8) account for how the interactions among

transition dipoles, in this case for the symmetric methyl stretch, are mediated by the excitation

mechanism. In an isotropic Raman transition, the oscillations of the isotropic polarizabilities of

all of the excited methyl groups are synchronized, regardless of orientation, and so the relevant

Legendre polynomial is $P_0(\cos \theta_{ij})$, which is equal to 1. For IR excitation, methyl groups that

are parallel oscillate in phase with one another, whereas methyl groups that are antiparallel

oscillate out of phase with one another. Methyl groups that are perpendicular to one another have

no phase relationship on average. In this case, the relevant Legendre polynomial is $P_1(\cos \theta_{ij})$,

which is $\cos \theta_{ij}$. For a depolarized Raman transition of a mode that is not completely

depolarized, such as the symmetric methyl stretch, the depolarized portions of the Raman tensor

of methyl groups that are parallel or antiparallel oscillate in phase with one another, whereas

those for molecules that are perpendicular oscillate out of phase with one another. The relevant

Legendre polynomial for this situation is $P_2(\cos \theta_{ij})$, which is $\frac{1}{2}(3 \cos^2 \theta_{ij} - 1)$.

Based on the above, it is clear that the excitation step in VSFG, which occurs via an IR transition, determines how the phase of the symmetric methyl stretch depends on orientation. Thus, regardless of whether the Raman transition is predominantly isotropic, depolarized, or some mixture of the two, the shift due to resonant coupling will be given by Eq. (7). It is important to note that the shift may change in the time between excitation of the vibration and the Raman probing step, but to a good approximation we can ignore this time dependence, as well as the time dependence in Eq. (9). It is also worth noting that in vibrational difference-frequency-generation (VDFG), the excitation occurs via a Raman transition, leading to different resonant coupling. Thus, comparison between VSFG and VDFG data for the same mode at the same interface could yield detailed information regarding resonant vibrational coupling.

Shown in Table 1 are the values of $\Delta\tilde{v}_{iso}$, $\Delta\tilde{v}_{IR}$, and $\Delta\tilde{v}_{dep}$ for the bulk liquid and for the interfacial liquid, as determined from our molecular simulations and Eqs. (6) – (8), based on the value of the methyl transition dipole that gives a value of 1.80 cm^{-1} for $\Delta\tilde{v}_{iso}$ in the bulk liquid. In the bulk liquid, we find that $\Delta\tilde{v}_{IR}$ is small and negative, which is consistent with the slight preference for antiparallel organization seen in Fig. 5B. Another manifestation of the slight preference for antiparallel organization is that $\Delta\tilde{v}_{dep}$ is small and positive.

Table 1

Spectral shifts for the methyl symmetric stretch calculated using Eqs (6) – (8) and assuming that the entire bulk isotropic shift upon isotopic dilution arises from resonant coupling. The estimated uncertainty in each shift is ±5%.

Medium	$\Delta\tilde{\nu}_{iso}$ (cm⁻¹)	$\Delta\tilde{\nu}_{IR}$ (cm⁻¹)	$\Delta\tilde{\nu}_{dep}$ (cm⁻¹)
Bulk	-1.80	-0.15	0.43
Bilayer, at least 1 molecule per pair	-1.79	0.65	0.27
Bilayer, both molecules	-0.72	1.90	0.11
First sublayer, at least 1 molecule per pair	-3.60	1.40	0.35
First sublayer, both molecules	1.90	1.01	0.22
Second sublayer, at least 1 molecule per pair	-5.04	2.07	0.14
Second sublayer, both molecules	1.59	0.65	0.04
Interlayer, normalized to first sublayer	-2.34	1.00	-0.02
Interlayer, normalized to second sublayer	-2.64	1.13	-0.02

To understand the sources of the resonant coupling, the calculated shifts for the interface were analyzed in a number of different scenarios. Shifts were calculated separately for the entire bilayer, and for each individual sublayer, based on at least one molecule in each pair being in that region and based on both molecules in each pair being in that region. The "interlayer" values were also calculated for one molecule being in each sublayer, normalized either to the number of molecules in the first sublayer or to the number of molecules in the second sublayer. Whether or not a molecule was in the bilayer, or in a specific sublayer, was determined based on the *z*

coordinates of its nitrogen and methyl carbon atoms. Molecules were considered to be in the first bilayer if the position of their methyl carbon atom was less than 4.35 Å in the *z* direction from the plane of the silanol oxygen atoms, based on the local minimum at this distance in the density profile for this atom, and following previous interpretations of the bilayer picture in acetonitrile [29]. The first sublayer of the first bilayer was defined based on the local minimum in the density profile for nitrogen at 2.39 Å, with the remaining molecules in the first bilayer considered as being in the second sublayer.

Although the results of the different analyses of the interfacial liquid vary somewhat, there are some clear trends apparent in Table 1. The value of $\Delta\tilde{\nu}_{iso}$ is negative in most cases, and has a magnitude on the order of 1 to several cm^{-1}. However, in the case that is likely the most physically realistic, in which the strongest coupling occurs when both molecules are in the same sublayer (see below), $\Delta\tilde{\nu}_{iso}$ is positive. The value of $\Delta\tilde{\nu}_{dep}$ is positive in nearly all cases, and is roughly an order of magnitude smaller on average than the value of $\Delta\tilde{\nu}_{iso}$. Importantly for the analysis of the VSFG data, $\Delta\tilde{\nu}_{IR}$ is positive in all cases, and takes on a value between roughly 0.65 and 2.07 cm^{-1}. The implication of $\Delta\tilde{\nu}_{IR}$ being positive at the interface is that resonant coupling would lead to a red shift of the VSFG spectrum upon isotopic dilution.

A comparison of the above analysis with experimental results from the bulk and the interface makes it clear that resonant coupling alone cannot be responsible for the observed blue shift of the VSFG spectrum upon isotopic dilution, given that our analysis shows that the shift in the VSFG spectrum due to resonant coupling is in the wrong direction. This observation also suggests that the value of the transition dipole for the methyl symmetric stretch is closer to the minimum value discussed above than the maximum value used here. That being said, for consistency, we will use the upper bound in the remaining plots in this paper.

It is intriguing that the magnitude of the VSFG blue shift at infinite dilution is less than that of the isotropic spectrum in the bulk liquid, which suggests that resonant coupling does play a measurable role in the shift in both environments. In this picture, repulsive interactions, in the form of caging, lead to a blue shift upon isotopic dilution in the bulk and interfacial liquids. Based on the different excitation mechanisms, our simulations suggest that resonant coupling shifts the bulk isotropic Raman spectrum to the blue by more than twice the amount that this mechanism shifts the *SSP* VSFG spectrum at the silica interface to the red.

The average IR shift for the two sublayers in the most likely case in Table 1 is 0.83 cm^{-1}. If we assume that the blue shift due to repulsive interactions is the same in the bulk and at the interface, but that the resonant coupling interactions need to be scaled down due to a lower transition dipole moment, the scaling factor comes out to be ~4.4, which is even larger than the scaling factor for the lower limit of the square of the transition dipole discussed above. If, on the other hand, we use the scaling factor of 3.5, i.e. use the transition dipole moment of Andrews and Boxer for acetonitrile-d_3 [40], then we find a blue shift due to repulsive interactions of 1.29 cm^{-1} for the bulk liquid and 1.44 cm^{-1} for the interface. Given the segregation of the methyl groups into the hydrophobic region of the surface layer, and the considerably higher density of methyl groups than in the bulk [34], a larger shift due to repulsive interactions at the interface is reasonable. These results suggest that the true magnitude of the methyl stretching transition dipole may indeed be near the lower limit.

The fact that the resonant coupling varies from molecule to molecule can lead to inhomogeneous broadening. To assess the extent of possible inhomogeneous broadening due to resonant coupling, in Figs. 6 to 8 we plot the probability distribution of the simulated shifts of the isotropic Raman, infrared, and depolarized Raman spectra of the methyl symmetric stretch

due to this mechanism in the bulk and in each of the sublayers of the interface, respectively (assuming, in the latter two cases, that only methyl groups within the same sublayer undergo resonant coupling). These calculations were performed in the upper limit that the entire shift in the isotropic Raman spectrum is due to resonant coupling; in the lower limit the shifts and standard deviations and full widths at half maximum (FWHMs) of the distributions should all be scaled down by a factor of 3.5. The standard deviations of the distributions of shifts in the bulk liquid are of the order of 2 cm^{-1} or more, with the isotropic Raman distribution being the broadest and the depolarized Raman distribution being the narrowest. The largest shifts observed have magnitudes of more than 10 cm^{-1}. These distributions exhibit notable asymmetry.

The degree of instantaneous inhomogeneous broadening in the two sublayers is roughly half of that in the bulk. The standard deviations in the second sublayer are somewhat smaller than those in the first sublayer, which is somewhat surprising given the greater disorder in the second sublayer. The distributions of shifts at the interface are also considerably more symmetric than those in the bulk.

We can gain insight into the degree of symmetry of the instantaneous shift distributions by making heat maps of Eqs. (6) – (8), as a function of the angle and distance between methyl transition dipoles, that are weighted by the corresponding angularly-resolved radial distribution function. Such plots are shown for the bulk liquid in Fig. S2 and for the interfacial bilayer in Fig. S3. At any given fixed distance between transition dipoles, the heat maps for the interface are roughly symmetric or antisymmetric about 90°, leading to relatively symmetric shift distributions. The heat maps for the bulk liquid have far less symmetry about 90°, particularly at short distances, which leads to the asymmetric instantaneous shift distributions.
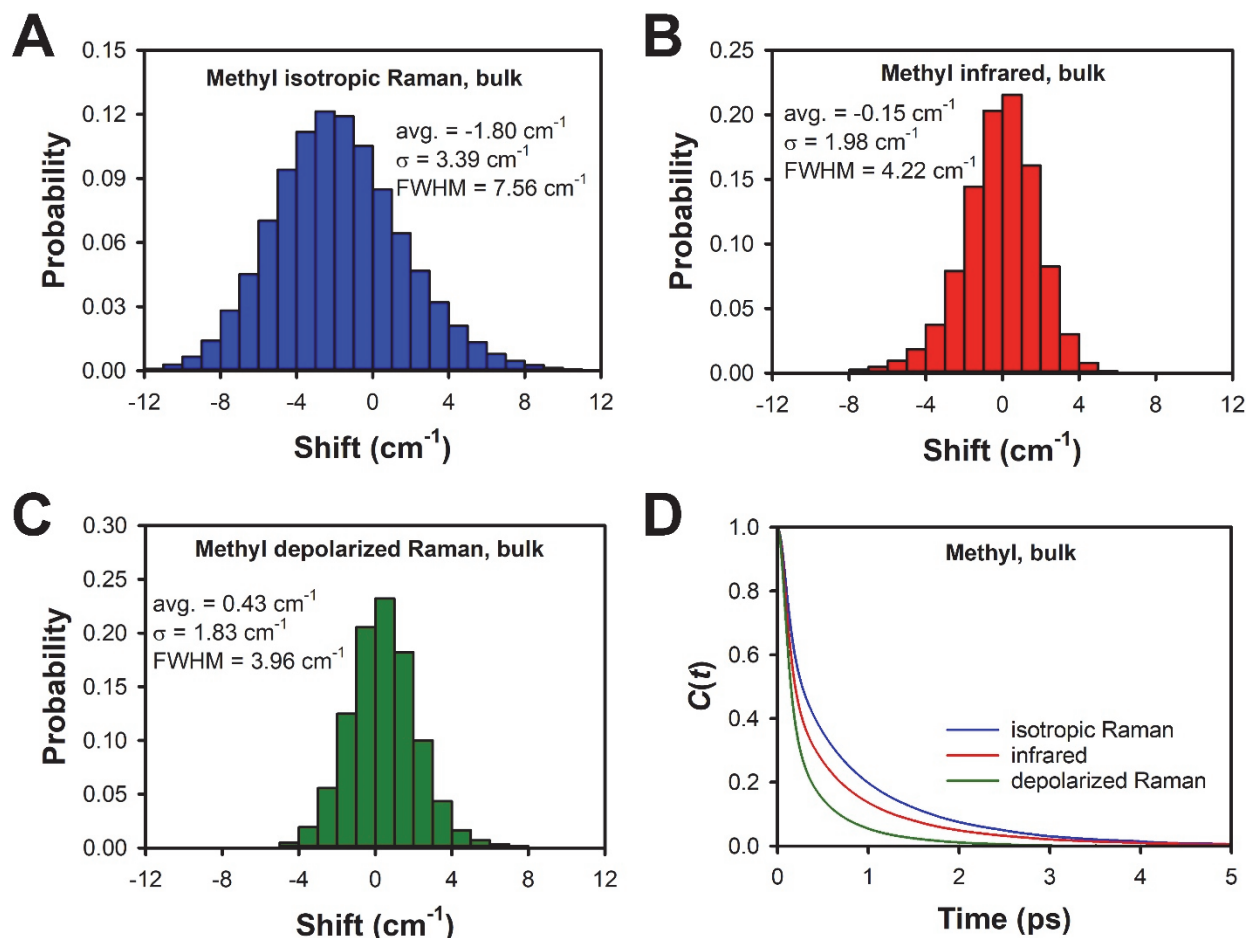
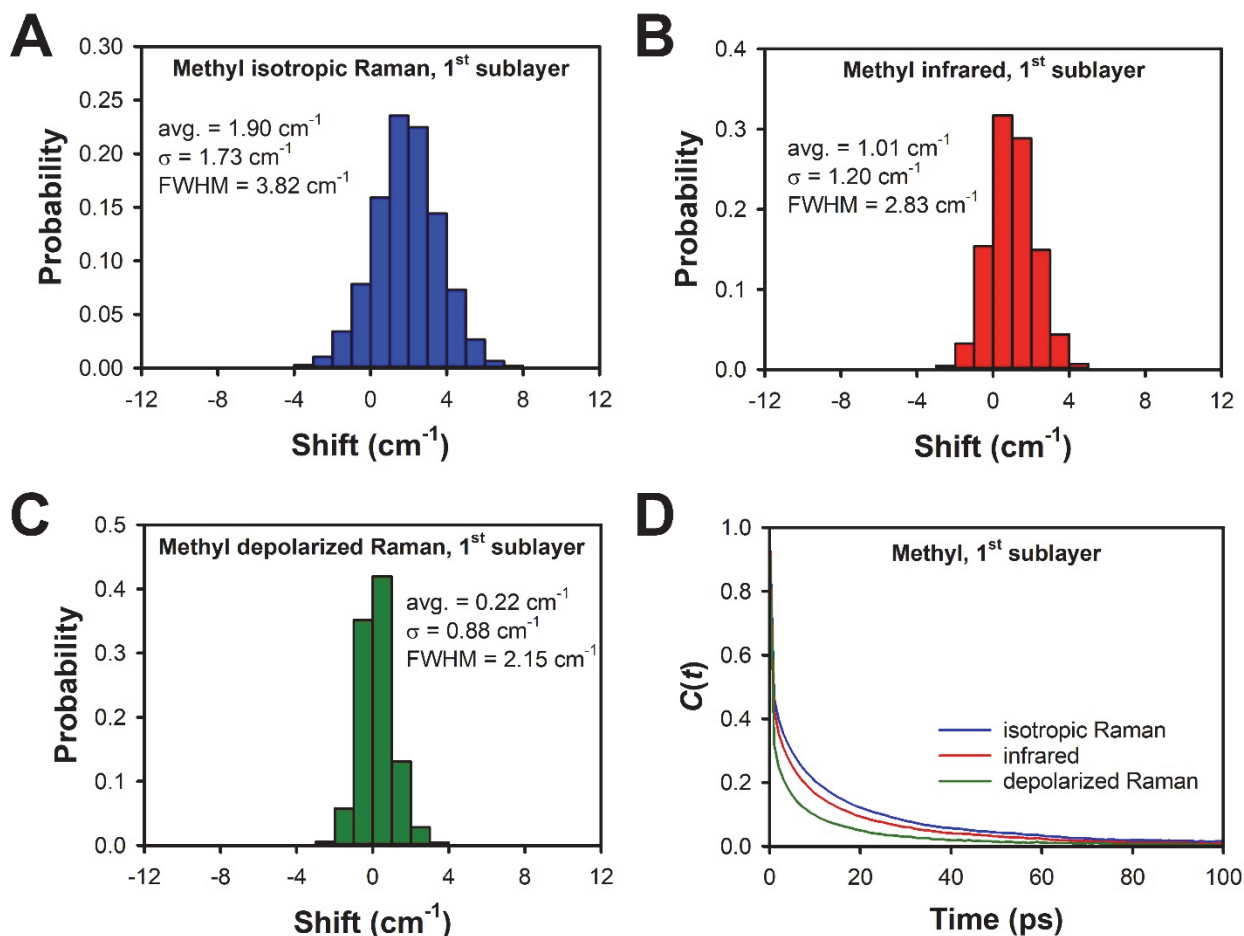**Fig. 6.** Instantaneous frequency shifts for the methyl symmetric stretch due to resonant coupling in bulk acetonitrile for (A) the isotropic Raman spectrum, (B) the infrared spectrum, and (C) the depolarized Raman spectrum. (D) The frequency correlation function for resonant coupling in the three different spectra. These plots assume the upper bound for the methyl symmetric stretch transition dipole. In the lower bound, the shifts and the widths of the shift distributions should be divided by ~3.5, but the correlation functions will be unchanged.
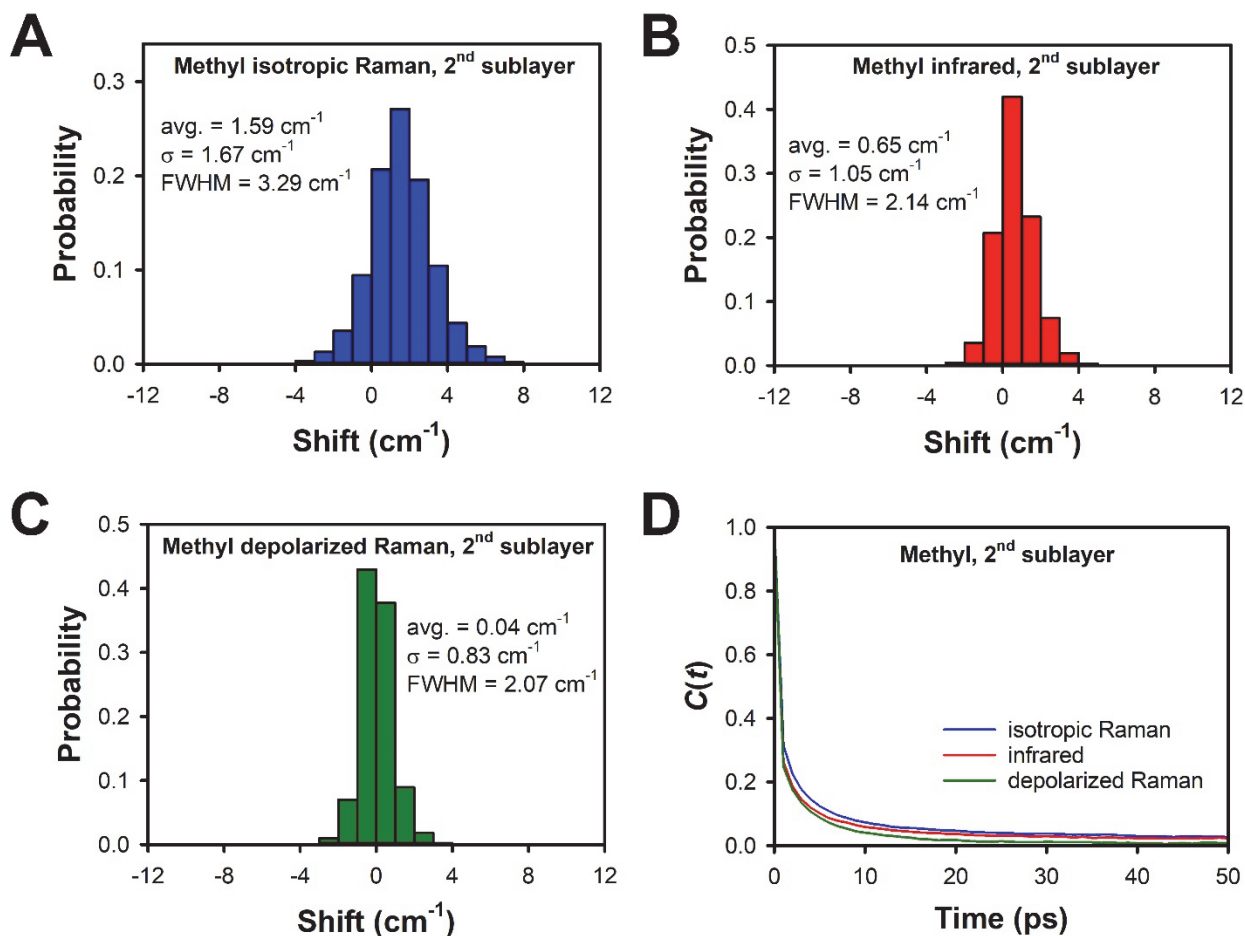
Fig. 7. Instantaneous frequency shifts for the methyl symmetric stretch due to resonant coupling in the first sublayer of acetonitrile at the silica/liquid interface for (A) the isotropic Raman spectrum, (B) the infrared spectrum, and (C) the depolarized Raman spectrum. (D) The frequency correlation function for resonant coupling in the three different spectra. These plots assume the upper bound for the methyl symmetric stretch transition dipole. In the lower bound, the shifts and the widths of the shift distributions should be divided by ~3.5, but the correlation functions will be unchanged.

Fig. 8. Instantaneous frequency shifts for the methyl symmetric stretch due to resonant coupling in the second sublayer of acetonitrile at the silica/liquid interface for (A) the isotropic Raman spectrum, (B) the infrared spectrum, and (C) the depolarized Raman spectrum. (D) The frequency correlation function for resonant coupling in the three different spectra. These plots assume the upper bound for the methyl symmetric stretch transition dipole. In the lower bound, the shifts and the widths of the shift distributions should be divided by ~3.5, but the correlation functions will be unchanged.

The above picture of inhomogeneous broadening due to resonant coupling is an instantaneous one. Having established the instantaneous probability distribution of shifts caused

by resonant coupling, we next explore how quickly the shift of any given molecule evolves. The shift due to resonant coupling is strongly dependent on the positions and orientations of the methyl groups of neighboring molecules, and if spectral diffusion occurs on a time scale faster than that of other dephasing mechanisms, then this process becomes a source of homogeneous dephasing, or even motional narrowing [77]. To quantify this effect, we calculated the time correlation function of the frequency shift due to resonant coupling:

$$C(t) = \sum_i \frac{\langle (\Delta\bar{v}(t) - \overline{\Delta\bar{v}})(\Delta\bar{v}(0) - \overline{\Delta\bar{v}}) \rangle}{\langle (\Delta\bar{v}(0) - \overline{\Delta\bar{v}})^2 \rangle} \ , \tag{10}$$

where $\overline{\Delta\bar{v}}$ is the average shift due to resonant coupling in a specific environment, i.e., the value shown in Table 1. In Figs. 6D, 7D, and 8D we plot $C_{iso}(t)$, $C_{IR}(t)$, and $C_{dep}(t)$ for the bulk liquid and the two sublayers at the silica/liquid interface, respectively. Assuming that the correlation functions can be described as a sum of exponentials, the average relaxation time is defined as

$$\tau_{av} = \int_0^\infty C(t)dt \ . \tag{11}$$

The average relaxation times for the bulk liquid are 0.64 ps for the isotropic Raman spectrum, 0.49 ps for the IR spectrum, and 0.29 ps for the depolarized Raman spectrum. Thus, the higher the order of the relevant Legendre polynomial, the more quickly the frequency shift time correlation function decays, in analogy with the behavior of orientational correlation functions [78]. In all cases the frequency correlation time is shorter than a typical vibrational dephasing time of a few picoseconds. The difference between these time scales is not large enough in the bulk liquid to be completely in the motionally narrowed regime, particularly for the isotropic Raman spectrum, but the transitions should at very least be considered to be homogeneously broadened as far as resonant coupling is concerned. Note that there are other mechanisms for

inhomogeneous broadening that could lead to even larger frequency shifts, and could have larger components that decay on a subpicosecond time scale. Such inhomogeneous contributions would be closer to, or even within, the motional narrowing limit. These results are consistent with Raman echo experiments that found no evidence for inhomogeneous broadening in the isotropic Raman spectrum of the bulk liquid [65]. Note that the frequency correlation functions are invariant to scaling, and so will be the same in the lower limit of the methyl transition dipole. However, the narrower distributions of instantaneous frequencies in that limit will lead to a narrower spectral contribution from resonant coupling.

As can be seen in Figs. 7D and 8D, the frequency correlation functions for the first and second sublayers at the silica surface both have a subpicosecond, Gaussian "ballistic" component, as well as a substantial component that decays on a time scale that is an order of magnitude or more slower than that of vibrational dephasing. The long spectral diffusion times are due to the fact that the dynamics at this interface are considerably slower than in the bulk liquid [58]. As would be expected, the frequency correlation time is longer in the first sublayer than in the second sublayer, because the latter layer has greater mobility. Thus, we can conclude that resonant coupling leads to inhomogeneous broadening in the VSFG spectrum of the symmetric methyl stretch. Indeed, the average interfacial inhomogeneous broadening due to resonant coupling of 0.66 cm^{-1} is similar to the experimental narrowing of the VSFG spectrum of 0.8 cm^{-1} upon isotopic dilution.

The largest shifts that can occur due to resonant coupling arise from nearest neighbors, and so isotopic dilution is expected to reduce inhomogeneous broadening by decreasing the number of nearest neighbors resonantly coupled to a given methyl group. To explore this phenomenon, we calculated the probability distribution of the instantaneous frequency shift again, but omitting

25%, 50%, and 75% of the methyl groups, chosen randomly, to mimic the effects of isotopic dilution on resonant coupling. The parameters describing the instantaneous shift distributions for the three spectra are shown in Fig. 9, along with the correlation functions for the isotropic spectrum. The other frequency correlation functions in the bulk, shown in Fig. S4, have a considerably weaker concentration dependence.

In the bulk liquid, the average shift and the width of the instantaneous shift distribution decrease, and the frequency correlation function decays more slowly, with increasing isotopic dilution for all three types of vibrational spectrum. Note that the actual increase in the correlation time is likely to be larger in the real liquid, because the simulations do not take into account the fact that the viscosity of acetonitrile-d_3 is ~9% greater than that of acetonitrile. As is evident from Fig. 9D, there are two qualitative trends in the frequency correlation function with increasing isotopic dilution, namely that the ballistic component decreases and the time scale of the slower component increases.

Above we concluded that the dominant mechanism for the blue shift in the isotropic Raman spectrum is repulsive interactions. However, this mechanism is sensitive to local composition, and so should lead to spectral broadening that depends on concentration, and reaches a maximum at a mole fraction of acetonitrile-d_3 nearer to 0.5 than to a mole fraction of 1.0 for either component [64]. As discussed above, the isotropic Raman linewidth is essentially independent of the concentration of acetonitrile-d_3. We should therefore consider whether the concentration dependence of resonant coupling can offset that of repulsive interactions. The fact that the width of the instantaneous inhomogeneous distribution of shifts decreases with increasing concentration of acetonitrile-d_3 could offset the increase in linewidth due to inhomogeneity in repulsive interactions at low concentrations of acetonitrile-d_3. The increase in the frequency

correlation time could lead to an increase of the linewidth due to resonant coupling at greater

dilutions. Coupled with the increased uncertainty in the linewidth at higher isotopic dilutions,

this effect could explain the experimental linewidth observations in the bulk liquid.
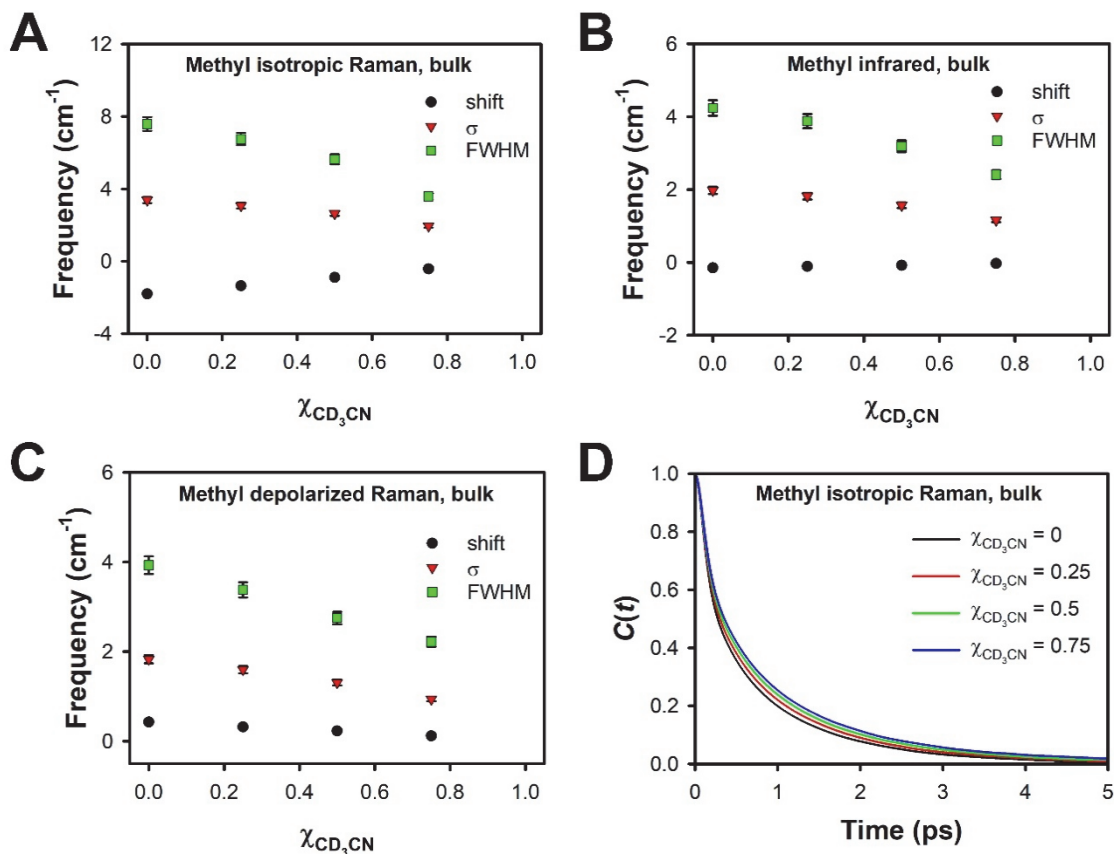

Fig. 9. Average instantaneous frequency shifts due to resonant coupling and the standard

deviation and FWHM of the frequency-shift distribution for the methyl symmetric stretch in the

bulk liquid as a function of the mole fraction of acetonitrile-d_3 for (A) the isotropic Raman

spectrum, (B) the infrared spectrum, and (C) the depolarized Raman spectrum. (D) The

frequency correlation functions for resonant coupling in the isotropic Raman spectrum for the

same isotopic dilutions. These plots assume the upper bound for the methyl symmetric stretch

transition dipole. In the lower bound, the shifts and the widths of the shift distributions should be

divided by ~3.5, but the correlation functions will be unchanged.

We next consider the two sublayers at the silica/liquid interface. The resonant coupling shift distributions and frequency correlation functions for the two sublayers are given in Figs. S5 – S8. Upon isotopic dilution, the frequency correlation functions for the two sublayers continue to decay on a time scale that is much longer than that of vibrational dephasing, such that the symmetric methyl stretch remains inhomogeneously broadened in the VSFG spectrum. However, the width of the instantaneous frequency shift distribution decreases upon isotopic dilution, which means that the inhomogeneous broadening also decreases, which is consistent with our experimental observations (Fig. 3B). These observations suggest why the VSFG intensity becomes greater than expected based on the mole fraction of acetonitrile as the isotopic dilution increases (Fig. 2B). The methyl symmetric stretches of molecules in the two sublayers have different frequencies, which leads to a substantial VSFG signal in this nearly cetrosymmetric system. Decreasing the inhomogeneous broadening of these two contributions decreases their spectral overlap, thereby increasing the overall VSFG signal.

The same molecular dynamics simulations can also be used to calculate the spectroscopic shifts in the C≡N stretch that arise from resonant coupling. The commonly proposed organization of liquid acetonitrile that involves dipole pairing of cyano groups [79] would be expected to lead to a significant Raman non-coincidence effect. However, experimental results show that the peak of the isotropic Raman spectrum is ~1 cm^{-1} to the red of the peak of the depolarized Raman spectrum in this liquid [39]. This result is consistent with our recent finding that antiparallel dimers in liquid acetonitrile are better described as octupole paired, i.e., that the molecules pair along their entire lengths, rather than via the cyano groups [37].

The C≡N stretch of acetonitrile is highly polarized, with a depolarization ratio on the order of 0.04 [80], and so the peak of the isotropic Raman spectrum should be at essentially the same

frequency as that of the polarized Raman spectrum, 2253.3 cm^{-1} [81]. The position of the peak of the IR spectrum is typically reported to be ~2254 cm^{-1} [82], although the determination of the peak frequency is complicated by the presence of a Fermi resonance [83].

Morales and Thompson [84] performed a detailed and insightful analysis of the gas-to-liquid frequency shift of the infrared spectrum of the acetonitrile C≡N stretch based on molecular dynamics simulations. They found that this shift is not dominated by specific pairs of molecules, but rather is largely an average over the molecules in the first solvation shell. They did not address the shifts among the IR spectrum and the isotropic and depolarized Raman spectra, but the many-body effects that they did consider are largely relevant to all three of these spectra.
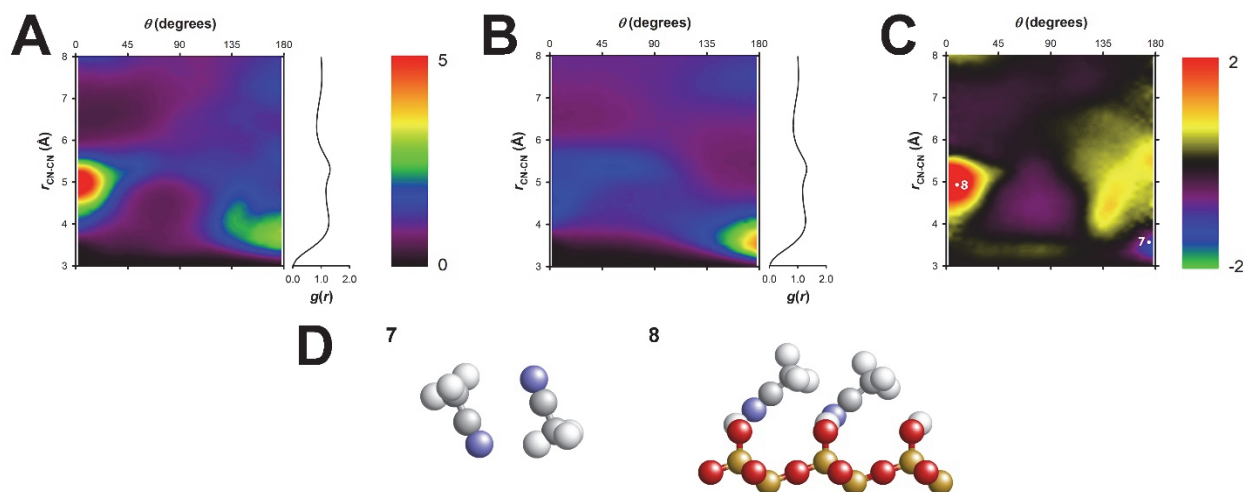

Fig. 10. Angularly-resolved radial distribution functions and radial distribution functions for the CN transition dipole in (A) the surface bilayer of acetonitrile at a silica interface and (B) bulk liquid acetonitrile. (C) A difference map between the angularly-resolved radial distribution functions for the interfacial bilayer and the bulk liquid, and (D) the representative pair configurations denoted in (C), including surface silanol groups for the interfacial pairs. The atom colors are the same as in Fig. 5. The color scale is the same for (A) and (B).

Fig. 10 shows the angularly-resolved radial distribution functions for the bulk and interfacial liquids, as well as the difference spectrum between the two. As expected, antiparallel cyano groups are more common in the bulk liquid (representative configuration 7), and parallel cyano groups are more common at the interface (representative configuration 8). The representative configuration at the interface exhibits on offset, head-to-tail structure that is reminiscent of pairing observed in the bulk liquid [37].

Table 2

Spectral shifts for the cyano stretch calculated using Eqs (6) – (8) and using the experimental value for the transition dipole moment [40]. The estimated uncertainty in each shift is ±5%.

Medium	$\Delta\tilde{v}_{iso}$ (cm^{-1})	$\Delta\tilde{v}_{IR}$ (cm^{-1})	$\Delta\tilde{v}_{dep}$ (cm^{-1})
Bulk	-1.23	0.40	-0.06
Bilayer, at least 1 molecule per pair	-1.10	0.52	-0.09
Bilayer, both molecules	-0.36	0.61	-0.07
First sublayer, at least 1 molecule per pair	-1.26	0.67	-0.12
First sublayer, both molecules	0.42	0.27	0.07
Second sublayer, at least 1 molecule per pair	-2.46	1.21	-0.29
Second sublayer, both molecules	0.31	0.15	0.02
Interlayer, normalized to first sublayer	-0.69	0.38	-0.11
Interlayer, normalized to second sublayer	-0.77	0.43	-0.12

The transition dipole has been reported to have a value of 0.058 D for the acetonitrile cyano stretch [40], which enables us to predict the resonant coupling spectral shifts directly from our simulations. These shifts are listed in Table 2. In the bulk liquid, the depolarized Raman peak is predicted to be shifted 1.17 cm^{-1} to the blue with respect to the isotropic Raman peak, in good agreement with experiment [39]. The comparison of the predicted 1.63 cm^{-1} shift of the IR spectrum with experimental measurements is more difficult to assess, as we were unable to find any single work in which careful measurements of the IR spectrum and at least one Raman spectrum were made. Additionally, the asymmetry of this peak due to other spectral features makes it difficult to ascertain the peak position accurately. Nevertheless, our results suggest that resonant coupling accounts for the majority of the differences among the shifts of these spectra for the C≡N stretch in the bulk liquid.

Table 2 also lists the calculated shifts for the cyano groups in the interfacial liquid, in the same combinations as used for the symmetric methyl stretch. Because hydrogen bonding to surface silanols will cause a substantial blue shift in the cyano stretch [83] for molecules in the first sublayer, again the most likely scenario is that there is little resonant coupling between the two sublayers. The shift of the VSFG spectrum due to resonant coupling is thus predicted to be 0.27 cm^{-1} in the first sublayer and 0.15 cm^{-1} in the second sublayer. These shifts are smaller than those found for the symmetric methyl stretch in the upper limit, but similar to those in the lower limit. This behavior can be understood readily based on Fig. 10. The most prominent feature at the interface is parallel cyano groups with a separation of ~5.0 Å, which is a large enough distance that the resonant coupling is weak. In contrast, the most prominent feature in the bulk

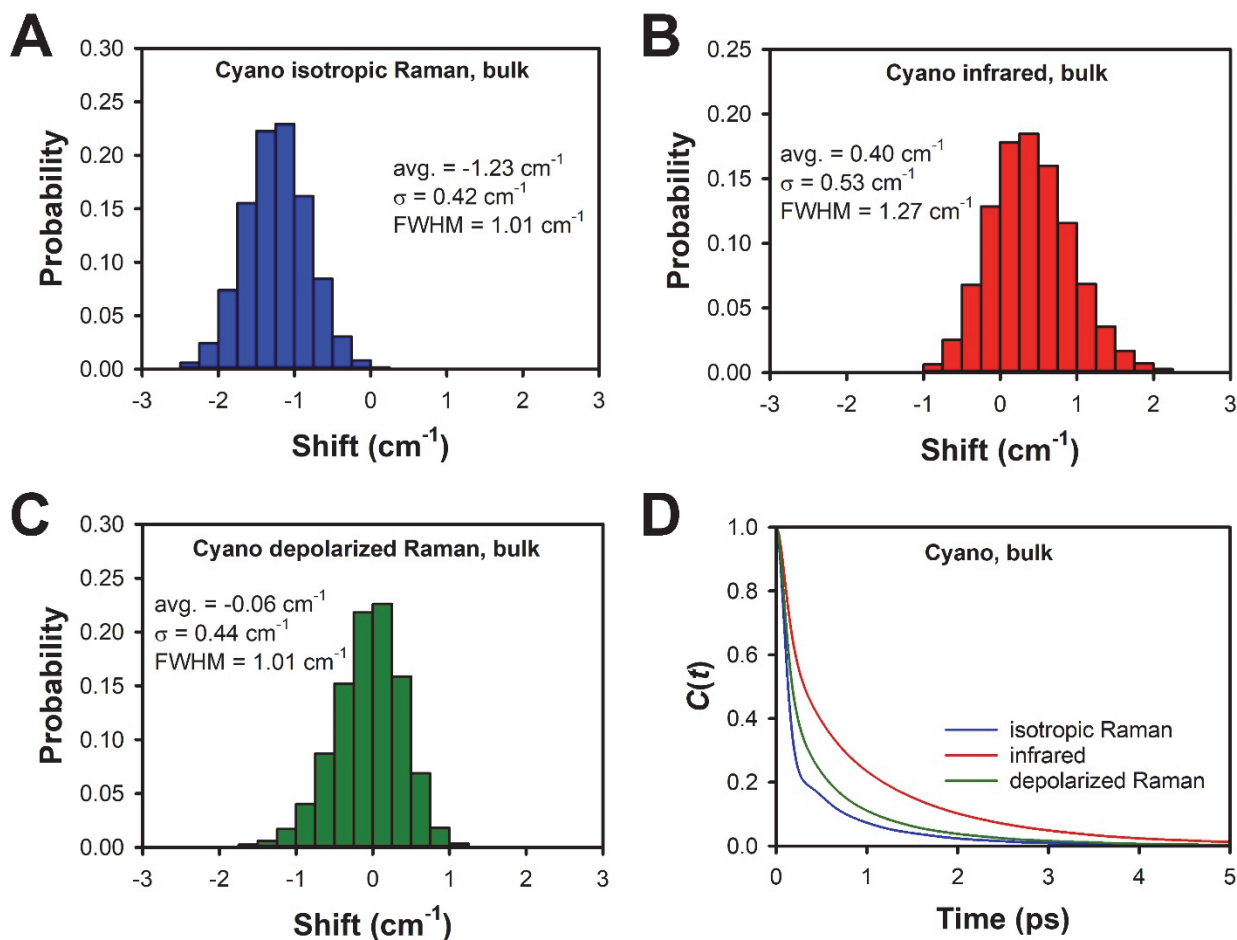liquid is antiparallel cyano groups with a separation of ~3.5 Å (Fig. 10B), enabling stronger resonant coupling.

Fig. 11. Instantaneous frequency shifts for the cyano stretch due to resonant coupling in bulk acetonitrile for (A) the isotropic Raman spectrum, (B) the infrared spectrum, and (C) the depolarized Raman spectrum. (D) The frequency correlation function for resonant coupling in the three different spectra.

The instantaneous shift distributions and frequency correlation functions for the bulk liquid are shown in Fig. 11, and the corresponding plots for the two sublayers are given in Figs. S9 and

S10. The FWHM of the instantaneous shift distribution for the cyano isotropic Raman spectrum, 1.07 cm^{-1}, is considerably narrower than that for the symmetric methyl stretch, 2.11 cm^{-1}, using the lower limit of the transition dipole moment for the mode. Comparison of Figs. 5B and 10B indicates that methyl groups take on a broad range of relative orientations at short distances, whereas cyano groups strongly favor an antiparallel relative orientation at short distances. Accordingly, the methyl symmetric stretch experiences a greater degree of instantaneous inhomogeneous broadening due to resonant coupling. A similar effect is observed for the shift distributions for the isotropic Raman spectrum for the two sublayers at the silica interface. The source of this behavior is apparent from Figs. 5A and 10A. Although the methyl groups have a preference for both parallel and antiparallel relative orientations in both sublayers, the cyano groups strongly favor parallel relative orientations in both sublayers.

Interestingly, the FWHMs of the shift distributions for the IR and depolarized Raman spectra are similar for both modes in all three environments investigated here. In the case of the methyl symmetric stretch, the IR and depolarized Raman shift distributions are narrower than the isotropic Raman shift distribution. On the other hand, for the cyano stretch in a given environment, the three shift distributions have similar widths. The source of this behavior can be gleaned from maps of Eqs. (6) – (8) weighted by the angularly-resolved radial distribution function for both modes (Figs. S2, S3, S11, and S12). The distance over which molecules contribute significantly to the potential is on the order of 6 Å for the symmetric methyl stretch, but only a bit greater than 4 Å for the cyano stretch. The number of methyl groups resonantly coupled to each methyl group is therefore larger than the number of cyano groups resonantly coupled to each cyano group, leading to a broader distribution of shifts in the methyl isotropic Raman spectrum. The regions with negative potentials for higher-order Legendre polynomials

shrink for the methyl stretch, reducing the range of shifts. The cyano potentials are dominated by a feature at ~3.5 Å for all of the Legendre polynomials, and so the width of the static shift distribution is relatively insensitive to the order of the Legendre polynomial.

In Fig. 11D we plot the frequency time correlation functions for the cyano stretch in the bulk liquid. The average decay times are 0.31 ps for the isotropic Raman spectrum, 0.74 ps for the IR spectrum, and 0.43 ps for the depolarized Raman spectrum. This ordering is different from that of the symmetric methyl stretch, in which the correlation time decreased with increasing order of the Legendre polynomial. In the isotropic Raman correlation function there is also a weak recurrence at a time of ~0.5 ps. There is a slight flattening in the corresponding methyl correlation function at about the same time (Fig. 6D), but the feature is considerably more prominent in the case of the cyano stretch. Because the largest contribution to this correlation function arises from antiparallel cyano groups, we speculate that this feature arises from librations in "octupole paired" dimers [37]. Given that the methyl groups in such dimers are substantially farther apart than the cyano groups, the effect of such motions is expected to be considerably weaker in the methyl symmetric stretch correlation functions.

As shown in Figs. S9D and S10D, in the first sublayer the ordering of the frequency correlation times matches that for the methyl symmetric stretch in all environments, whereas in the second sublayer the ordering matches that for the bulk liquid. The anomalous ordering of the cyano frequency correlation times in the bulk can also be explained using the maps of Eqs. (6) – (8). In the case of the IR spectrum, the shifts in both the parallel and antiparallel regions of the map are positive, which means that a reorientation of 180° does not cause a substantial frequency shift. For the isotropic and depolarized Raman spectra, the shifts are of opposite sign for parallel and antiparallel orientations, and so a reorientation of 180° changes the sign of the shift. In the

first sublayer, the cyano groups are essentially unable to undergo 180° reorientations, and so the behavior is determined largely by the order of the Legendre polynomial. The more mobile second sublayer acts much in the same way as the bulk liquid.

4. Conclusions

We have presented a VSFG study of the methyl symmetric stretch of liquid acetonitrile at a silica interface for a series of mixtures of acetonitrile with its fully deuterated isotopologue. We were able to obtain spectra down to an acetonitrile mole fraction of 0.05, and to resolve small changes in line shape. The VSFG spectra exhibit a blue shift and a narrowing with isotopic dilution, and the intensity of the spectrum is higher than predicted, particularly at low acetonitrile concentrations. Molecular dynamics simulations show that these spectral changes are consistent with the presence of resonant intermolecular vibrational coupling, although the dominant mechanism for the frequency shift appears to be repulsive interactions. The resonant coupling for the methyl group is found to be on the same order as that in the bulk liquid. We have further demonstrated that it is the position of the IR transition that determines how resonant coupling influences the VSFG spectrum. The IR shift in the symmetric methyl stretch due to resonant coupling is substantially larger in VSFG spectroscopy than that in the bulk liquid, and has the opposite sign.

Our molecular simulations also clarify the behavior of the isotropic Raman spectrum of the symmetric methyl stretch of acetonitrile upon isotopic dilution. The observed blue shift arises from a combination of repulsive interactions and resonant coupling. The fact that the isotropic Raman linewidth is independent of the mole fraction of acetonitrile-d_3 appears to arise from the opposite influence of the two shift mechanisms on the linewidth upon isotopic dilution. The

ability of resonant coupling to decrease linewidths with increasing isotopic dilution that was observed here is likely to be general.

Based on our simulations and the known transition dipole for the acetonitrile cyano stretch, we are able to reproduce the Raman non-coincidence effect for this mode in the bulk liquid. Calculations for the acetonitrile cyano stretch at the same interface suggest a resonant coupling shift of the same general magnitude as that of the symmetric methyl stretch. In the case of the cyano stretch, the IR frequency shift due to resonant coupling is smaller at the interface than in the bulk liquid. The different organizations of the methyl groups and cyano groups, both in the bulk liquid and at the interface, lead to anomalous behavior in the frequency correlation functions for the cyano stretch in the bulk and the second sublayer, in which the correlation time does not decrease with increasing order of the relevant Legendre polynomial.

Our results indicate that the organization imposed upon a liquid by an interface can either increase or decrease resonant coupling between vibrations, and that within the same molecule the effect of this structuring on the magnitude of resonant coupling in different vibrational modes need not be the same. Although the methyl symmetric stretches and cyano stretches studied here are not fully in the excitonic regime in this system, it is clear from our results that functional groups with larger transition-dipole moments could be driven entirely into this regime at interfaces. With this idea in mind, it would be of great interest, for instance, to perform similar experiments using carbonyl stretches at interfaces as a probe of resonant coupling. As an example, although the dipole moments of carbonyl groups tend to lead to antiparallel local ordering in the bulk [85], parallel ordering may be enforced at an interface, leading to a substantial change in resonant coupling.

Although the resonant coupling studied here does not fully reach the excitonic regime, the magnitude is still large enough to lead to excitation hopping. This phenomenon can mimic reorientation, and at an interface with slow reorientational dynamics could be substantially faster than reorientation. In the presence of such hopping, models that are used to determine orientational distributions from VSFG spectra will not give accurate results [6]. Our results suggest that the effects of resonant coupling should generally be considered when analyzing VSFG spectra at solid/liquid interfaces, and likely in other situations, such as liquid/liquid interfaces, as well.

CRediT authorship contribution statement

Amanda J. Souna: Formal analysis, Investigation, Writing – original draft, Writing – review & editing. Samuel R. Cohen: Conceptualization, Formal analysis, Investigation Formal analysis, Investigation, Visualization, Writing – original draft, Writing – review & editing. Christopher A. Rivera: Conceptualization, Formal analysis, Investigation. Katherine Manfred: Formal analysis, Investigation. Benoit Coasne: Conceptualization, Supervision, Writing – review & editing. John T. Fourkas: Conceptualization, Formal analysis, Funding acquisition, Project administration, Supervision, Visualization, Writing – review & editing.

Declaration of Competing Interest

The authors declare that they have no known competing financial interests or personal relationships that could have appeared to influence the work reported in this paper.

References

[1] M. Buck, M. Himmelhaus, Vibrational Spectroscopy of Interfaces by Infrared-Visible Sum Frequency Generation, J. Vac. Sci. A 19 (2001) 2717.

[2] K.B. Eisenthal, Liquid Interfaces Probed by Second-Harmonic and Sum-Frequency Spectroscopy, Chem. Rev. 96 (1996) 1343.

[3] F. Vidal, A. Tadjeddine, Sum-Frequency Generation Spectroscopy of Interfaces, Rep. Prog. Phys. 68 (2005) 1095.

[4] H.F. Wang, W. Gan, R. Lu, Y. Rao, B.H. Wu, Quantitative Spectral and Orientational Analysis in Surface Sum Frequency Generation Vibrational Spectroscopy (Sfg-Vs), Int. Rev. Phys. Chem. 24 (2005) 191.

[5] G.L. Richmond, Molecular Bonding and Interactions at Aqueous Surfaces as Probed by Vibrational Sum Frequency Spectroscopy, Chem. Rev. 102 (2002) 2693.

[6] C.A. Rivera, J.T. Fourkas, Reexamining the Interpretation of Vibrational Sum-Frequency Generation Spectra, Int. Rev. Phys. Chem. 30 (2011) 409.

[7] P.N. Butcher, D. Cotter, The Elements of Nonlinear Optics. Cambridge University Press, Cambridge, 1990.

[8] H. Chen, W. Gan, B.H. Wu, D. Wu, Z. Zhang, H.F. Wang, Determination of the Two Methyl Group Orientations at Vapor/Acetone Interface with Polarization Null Angle Method in Sfg Vibrational Spectroscopy, Chem. Phys. Lett. 408 (2005) 284.

[9] R. Lu, W. Gan, H.F. Wang, Novel Method for Accurate Determination of the Orientational Angle of Interfacial Chemical Groups, Chin. Sci. Bull. 48 (2003) 2183.

[10] E. Tyrode, C.M. Johnson, S. Baldelli, C. Leygraf, M.W. Rutland, A Vibrational Sum Frequency Spectroscopy Study of the Liquid−Gas Interface of Acetic Acid−Water Mixtures: 2. Orientation Analysis, J. Phys. Chem. B 109 (2004) 329.

[11] D. Zhang, J. Gutow, K.B. Eisenthal, Vibrational-Spectra, Orientations, and Phase-Transitions in Long-Chain Amphiphiles at the Air-Water-Interface - Probing the Head and Tail Groups by Sum-Frequency Generation, J. Phys. Chem. 98 (1994) 13729.

[12] J.T. Fourkas, R.A. Walker, S.Z. Can, E. Gershgoren, Effects of Reorientation in Vibrational Sum-Frequency Spectroscopy, J. Phys. Chem. C 111 (2007) 8902.

[13] S. Malyk, F.Y. Shalhout, L.E. O'Leary, N.S. Lewis, A.V. Benderskii, Vibrational Sum Frequency Spectroscopic Investigation of the Azimuthal Anisotropy and Rotational Dynamics of Methyl-Terminated Silicon(111) Surfaces, J. Phys. Chem. C 117 (2013) 935.

[14] M. Vinaykin, A.V. Benderskii, Orientational Dynamics in Sum Frequency Spectroscopic Line Shapes, J. Phys. Chem. B 117 (2013) 15833.

[15] X. Wei, Y.R. Shen, Motional Effect in Surface Sum-Frequency Vibrational Spectroscopy, Phys. Rev. Lett. 86 (2001) 4799.

[16] C.A. Rivera, A.J. Souna, J.S. Bender, K. Manfred, J.T. Fourkas, Reorientation-Induced Spectral Diffusion in Vibrational Sum-Frequency-Generation Spectroscopy., J. Phys. Chem. B 117 (2013) 15875.

[17] D.-S. Zheng, Y. Wang, A.-A. Liu, H.-F. Wang, Microscopic Molecular Optics Theory of Surface Second Harmonic Generation and Sum-Frequency Generation Spectroscopy Based on the Discrete Dipole Lattice Model, Int. Rev. Phys. Chem. 27 (2008) 629.

[18] M. Sass, J. Lobau, M. Lettenberger, A. Laubereau, Vibrational Energy Transfer of Chemisorbed Ethyltrichlorosilane at the Glass/Air Interface, Chem. Phys. Lett. 311 (1999) 13.

[19] S. Yamamoto, A. Ghosh, H.K. Nienhuys, M. Bonn, Ultrafast Inter- and Intramolecular Vibrational Energy Transfer between Molecules at Interfaces Studied by Time- and Polarization-Resolved Sfg Spectroscopy, Phys. Chem. Chem. Phys. 12 (2010) 12909.

[20] M. Bonn, C. Hess, M. Wolf, The Dynamics of Vibrational Excitations on Surfaces: Co on Ru(001), J. Chem. Phys. 115 (2001) 7725.

[21] J.A. McGuire, Y.R. Shen, Ultrafast Vibrational Dynamics at Water Interfaces, Science 313 (2006) 1945.

[22] J. Schaefer, E.H.G. Backus, Y. Nagata, M. Bonn, Both Inter- and Intramolecular Coupling of O-H Groups Determine the Vibrational Response of the Water/Air Interface, J. Phys. Chem. Lett. 7 (2016) 4591.

[23] W.J. Smit, J. Versluis, E.H.G. Backus, M. Bonn, H.J. Bakker, Reduced near-Resonant Vibrational Coupling at the Surfaces of Liquid Water and Ice, J. Phys. Chem. Lett. 9 (2018) 1290.

[24] A.M. Ricks, C.L. Anfuso, W. Rodriguez-Cordoba, T.Q. Lian, Vibrational Relaxation Dynamics of Catalysts on TiO_2 Rutile (110) Single Crystal Surfaces and Anatase Nanoporous Thin Films, Chem. Phys. 422 (2013) 264.

[25] J.O. Hirschfelder, C.F. Curtiss, R.B. Bird, Molecular Theory of Gases and Liquids. John Wiley & Sons, New York, 1954.

[26] M.G. Giorgini, Raman Noncoincidence Effect: A Spectroscopic Manifestation of the Intermolecular Vibrational Coupling in Dipolar Molecular Liquids, Pure Appl. Chem. 76 (2004) 157.

[27] D.E. Logan, The Non-Coincidence Effect in the Raman Spectra of Polar Liquids, Chem. Phys. 103 (1986) 215.

[28] C.H. Wang, J. McHale, Vibrational Resonance Coupling and the Noncoincidence Effect of the Isotropic and Anisotropic Raman Spectral Components in Orientationally Anisometric Molecular Liquids, J. Chem. Phys. 72 (1980) 4039.

[29] Z. Hu, J.D. Weeks, Acetonitrile on Silica Surfaces and at Its Liquid-Vapor Interface: Structural Correlations and Collective Dynamics, J. Phys. Chem. C 114 (2010) 10202.

[30] F. Ding, Z. Hu, Q. Zhong, K. Manfred, R.R. Gattass, M.R. Brindza, J.T. Fourkas, R.A. Walker, J.D. Weeks, Interfacial Organization of Acetonitrile: Simulation and Experiment, J. Phys. Chem. C 114 (2010) 17651.

[31] C.M. Morales, W.H. Thompson, Simulations of Infrared Spectra of Nanoconfined Liquids: Acetonitrile Confined in Nanoscale, Hydrophilic Silica Pores, J. Phys. Chem. A 113 (2009) 1922.

[32] L. Cheng, J.A. Morrone, B.J. Berne, Structure and Dynamics of Acetonitrile Confined in a Silica Nanopore, J. Phys. Chem. C 116 (2012) 9582.

[33] R.D. Mountain, Molecular Dynamics Simulation of Water-Acetonitrile Mixtures in a Silica Slit, J. Phys. Chem. C 117 (2013) 3923.

[34] J.W. Polster, A.J. Souna, M.H. Motevaselian, R.A. Lucas, J.D. Tran, Z.S. Siwy, N.R. Aluru, J.T. Fourkas, The Electrical-Double Layer Revisited, Nat. Sci. 2 (2022) e20210099.

[35] B.J. Loughnane, R.A. Farrer, A. Scodinu, J.T. Fourkas, Dynamics of a Wetting Liquid in Nanopores: An Optical Kerr Effect Study of the Dynamics of Acetonitrile Confined in Sol-Gel Glasses, J. Chem. Phys. 111 (1999) 5116.

[36] H. Saito, Y. Tanaka, S. Nagata, K. Nukada, [13]c Nuclear Magnetic Resonance Studies on Molecular Association. I. Self-Association of Dipolar Molecules, Can. J. Chem. 51 (1973) 2118.

[37] S.R. Cohen, M. Plazanet, S. Rols, D.J. Voneshen, J.T. Fourkas, B. Coasne, Structure and Dynamics of Acetonitrile: Molecular Simulation and Neutron Scattering, J. Mol. Liq. 348 (2022) 118423.

[38] V.A. Koverga, O.M. Korsun, O.N. Kalugin, B.A. Marekha, A. Idrissi, A New Potential Model for Acetonitrile: Insight into the Local Structure Organization, J. Mol. Liq. 233 (2017) 251.

[39] G. Fini, P. Mirone, Short-Range Orientation Effects in Dipolar Aprotic Liquids—Iii. Intermolecular Coupling of Vibrations in Sulfoxides, Sulfones, Nitriles and Other Compounds, Spectrochim. Acta A 32 (1976) 625.

[40] S.S. Andrews, S.G. Boxer, Vibrational Stark Effects of Nitriles I. Methods and Experimental Results, J. Phys. Chem. A 104 (2000) 11853.

[41] B.J. Berne, J.T. Fourkas, R.A. Walker, J.D. Weeks, Nitriles at Silica Interfaces Resemble Supported Lipid Bilayers, Acc. Chem. Res. 49 (2016) 1605.

[42] F. Ding, Q. Zhong, M.R. Brindza, J.T. Fourkas, R.A. Walker, Ti:Sapphire, Broadband Vibrational Sum-Frequency Generation Spectrometer with a Counter-Propagating Geometry, Opt. Express 17 (2009) 14665.

[43] V.V. Lozovoy, I. Pastirk, M. Dantus, Multiphoton Intrapulse Interference. Iv. Ultrashort Laser Pulse Spectral Phase Characterization and Compensation., Opt. Lett. 29 (2004) 775.

[44] A.J. Souna, J.S. Bender, J.T. Fourkas, How Clean Is the Solvent You Use to Clean Your Optics? A Vibrational Sum-Frequency-Generation Study, Appl. Opt. 56 (2017) 3875.

[45] A.M. Nikitin, A.P. Lyubartsev, New Six-Site Acetonitrile Model for Simulations of Liquid Acetonitrile and Its Aqueous Mixtures, J. Comput. Chem. 28 (2007) 2020.

[46] S. Plimpton, Fast Parallel Algorithms for Short-Range Molecular Dynamics, J. Comput. Phys. 117 (1995) 1.

[47] T.R. Forester, W. Smith, Shake, Rattle, and Roll: Efficient Constraint Algorithms for Linked Rigid Bodies, J. Comput. Chem. 19 (1998) 102.

[48] S.H. Lee, P.J. Rossky, A Comparison of the Structure and Dynamics of Liquid Water at Hydrophobic and Hydrophilic Surfaces—a Molecular Dynamics Simulation Study, J. Chem. Phys. 100 (1994) 3334.

[49] L. Martínez, R. Andrade, E.G. Birgin, J.M. Martínez, Packmol: A Package for Building Initial Configurations for Molecular Dynamics Simulations, J. Comput. Chem. 30 (2009) 2157.

[50] S. Nosé, A Unified Formulation of the Constant Temperature Molecular Dynamics Methods, J. Chem. Phys. 81 (1984) 511.

[51] D. Frenkel, B. Smit, Understanding Molecular Simulation: From Algorithms to Applications. 2nd edn. Academic Press, San Diego, 2002.

[52] Y.-P. Wang, K. Ren, S. Liu, The Joint Effect of Surface Polarity and Concentration on the Structure and Dynamics of Acetonitrile Solution: A Molecular Dynamics Simulation Study, Phys. Chem. Chem. Phys. 22 (2020) 10322.

[53] J.D. Weeks, D. Chandler, H.C. Andersen, Role of Repulsive Forces in Determining the Equilibrium Structure of Simple Liquids, J. Chem. Phys. 54 (1971) 5237.

[54] C.A. Rivera, J.S. Bender, K. Manfred, J.T. Fourkas, Persistence of Acetonitrile Bilayers at the Interface of Acetonitrile/Water Mixtures with Silica, J. Phys. Chem. A 117 (2013) 12060.

[55] A.J. Souna, T.L. Clark, J.T. Fourkas, Effect of Temperature on the Organization of Acetonitrile at the Silica/Liquid Interface, J. Phys. Chem. C 121 (2017) 26432.

[56] J. Kim, K.C. Chou, G.A. Somorjai, Structure and Dynamics of Acetonitrile at the Air/Liquid Interface of Binary Solutions Studied by Infrared−Visible Sum Frequency Generation, J. Phys. Chem. B 107 (2003) 1592.

[57] B.J. Loughnane, A. Scodinu, R.A. Farrer, J.T. Fourkas, U. Mohanty, Exponential Intermolecular Dynamics in Optical Kerr Effect Spectroscopy of Small-Molecule Liquids, J. Chem. Phys. 111 (1999) 2686.

[58] S.L. Liu, J.T. Fourkas, Orientational Time Correlation Functions for Vibrational Sum-Frequency Generation. 1. Acetonitrile, J. Phys. Chem. A 117 (2013) 5853.

[59] B.P. Asthana, V. Deckert, M.K. Shukla, W. Kiefer, Isotopic Dilution Study of Self Association in (Ch3cn+Cd3cn) Mixture by Scanning Multichannel Raman Difference Technique and Ab-Initio Calculations, Chem. Phys. Lett. 326 (2000) 123.

[60] K. Kamogawa, T. Kitagawa, Raman Difference Spectroscopy of the C-H Stretching Vibrations: Frequency Shifts and Excess Quantities for Acetone/Water and Acetonitrile/Water Solutions, J. Phys. Chem. 90 (1986) 1077.

[61] K. Kamogawa, T. Kitagawa, A New Device for Raman Difference Spectroscopy and Its Application to Observe Frequency Shifts Due to Isotope Mixing, J. Phys. Chem. 94 (1990) 3916.

[62] E. Marri, A. Morresi, G. Paliani, R.S. Cataliotti, M.G. Giorgini, Isotopic and Chemical Dilution Effects on the Vibrational Relaxation Rate of Some Totally Symmetric Motions of Liquid Acetonitrile, Chem. Phys. 243 (1999) 323.

[63] A. Morresi, M. Ombelli, P. Sassi, S. Santini, Light and Deuterated Acetonitrile: An Unresolved Casus?, J. Raman Spectrosc. 33 (2002) 71.

[64] E.W. Knapp, S.F. Fischer, The Concentration Dependence of the Vibrational Linewidth and Shift in Liquid Binary Mixtures: An Analytical Model, J. Chem. Phys. 76 (1982) 4730.

[65] D. Vanden Bout, L.J. Muller, M. Berg, Ultrafast Raman Echoes in Liquid Acetonitrile, Phys. Rev. Lett. 67 (1991) 3700.

[66] L.J. Muller, D.V. Bout, M. Berg, Broadening of Vibrational Lines by Attractive Forces: Ultrafast Raman Echo Experiments in a Ch3i:Cdcl3 Mixture, J. Chem. Phys. 99 (1993) 810.

[67] D. Ben-Amotz, M.R. Lee, S.Y. Cho, D.J. List, Solvent and Pressure-Induced Perturbations of the Vibrational Potential Surface of Acetonitrile, J. Chem. Phys. 96 (1992) 8781.

[68] P.S. Nikam, L.N. Shirsat, M. Hasan, Density and Viscosity Studies of Binary Mixtures of Acetonitrile with Methanol, Ethanol, Propan-1-Ol, Propan-2-Ol, Butan-1-Ol, 2-Methylpropan-1-

Ol, and 2-Methylpropan-2-Ol at (298.15, 303.15, 308.15, and 313.15) K, J. Chem. Eng. Data 43 (1998) 732.

[69] W.G. Killian, A.T. Norfleet, C.T. Lira, Densities of Selected Deuterated Solvents, J. Chem. Eng. Data 67 (2022) 893.

[70] R. Kopelman, Benzene Vibrational Exciton Spectrum, J. Chem. Phys. 47 (1967) 3227.

[71] J.E. Bertie, Y. Apelblat, C.D. Keefe, Infrared Intensities of Liquids Xxv: Dielectric Constants, Molar Polarizabilities and Integrated Intensities of Liquid Toluene at 25 °C between 4800 and 400 Cm^{-1}, J. Mol. Struct. 750 (2005) 78.

[72] N. Biliškov, Infrared Optical Constants, Molar Absorption Coefficients, Dielectric Constants, Molar Polarisabilities, Transition Moments and Dipole Moment Derivatives of Liquid N,N-Dimethylacetamide-Carbon Tetrachloride Mixtures, Spectrochim. Acta A 79 (2011) 295.

[73] N. Biliškov, Infrared Optical Constants, Molar Absorption Coefficients, Dielectric Constants, Molar Polarisabilities, Transition Moments and Dipole Moment Derivatives of Liquid N,N-Dimethylformamide-Carbon Tetrachloride Mixtures, Spectrochim. Acta A 79 (2011) 302.

[74] C.D. Keefe, J.E. Pickup, Infrared Optical Constants, Dielectric Constants, Molar Polarizabilities, Transition Moments, Dipole Moment Derivatives and Raman Spectrum of Liquid Cyclohexane, Spectrochim. Acta A 72 (2009) 947.

[75] J.A. Koningstein, Introduction to the Theory of the Raman Effect. Reidel, Dordrecht, 1972.

[76] O. Quinet, B. Champagne, V. Rodriguez, Experimental and Theoretical Investigation of the Raman and Hyper-Raman Spectra of Acetonitrile and Its Derivatives, J. Chem. Phys. 124 (2006) 244312.

[77] R. Kubo, Generalized Cumulant Expansion Method, J. Phys. Soc. Jpn. 17 (1962) 1100.

[78] B.J. Berne, R. Pecora, Dynamic Light Scattering: With Applications to Chemistry, Biology, and Physics. Dover Publications, Inc, Mineola, NY, 2000.

[79] J.E. Griffiths, Molecular Reorientational Motion in Liquid Acetonitrile: Raman Band Shapes, Diffusion Constants and Activation Energy of Reorientation, J. Chem. Phys. 59 (1973) 751.

[80] D. Bhattacharjee, A.G. , T.N. Misra, S.K. Nandy, Raman Spectral Study of Vibrational Relaxation of the Cn Stretching Band of Acetonitrile and Benzonitrile, J. Raman Spectrosc. 27 (1996) 457.

[81] F.H. Tukhvatullin, A. Jumabaev, G. Muradov, H.A. Hushvaktov, A.A. Absanov, Raman Spectra of Cn Vibrations of Acetonitrile in Aqueous and Other Solutions. Experimental Results and Ab Initio Calculations, J. Raman Spectrosc. 36 (2005) 932.

[82] S. Hashimoto, T. Ohba, S.-i. Ikawa, Infrared and Molecular Dynamics Study of Reorientational Relaxation of Liquid Acetonitrile, Chem. Phys. 138 (1989) 63.

[83] W.R. Fawcett, G. Liu, T.E. Kessler, Solvent-Induced Frequency Shifts in the Infrared Spectrum of Acetonitrile in Organic Solvents, J. Phys. Chem. 97 (1993) 9293.

[84] C.M. Morales, W.H. Thompson, Molecular-Level Mechanisms of Vibrational Frequency Shifts in a Polar Liquid, J. Phys. Chem. B 115 (2011) 7597.

[85] T.F. Sun, J.B. Chan, S.L. Wallen, J. Jonas, Raman Noncoincidence Effect of the Carbonyl Stretching Mode in Compressed Liquid Cyclic Carbonates, J. Chem. Phys. 94 (1991) 7486.